Full title

Short-range interactions between fibrocytes and CD8$^+$ T cells in COPD bronchial inflammatory response

Authors

Edmée Eyraud[1,2], Elise Maurat[1,2], Jean-Marc Sac-Epée[3], Pauline Henrot[1,2,4], Maeva Zysman[1,2,4], Pauline Esteves[1,2], Thomas Trian[1,2], Jean-William Dupuy[1], Alexander Leipold[4], Antoine-Emmanuel Saliba[4], Hugues Bégueret[1,2,5], Pierre-Oliver Girodet[1,2,5], Matthieu Thumerel[1,2,5], Romain Hustache-Castaing[1,2,5], Roger Marthan[1,2,5], Florian Levet[6,7], Pierre Vallois[3], Cécile Contin-Bordes[8,9], Patrick Berger[1,2,5], Isabelle Dupin[1,2,*]

Affiliations

[1]Univ-Bordeaux, Centre de Recherche Cardio-thoracique de Bordeaux, U1045, Département de Pharmacologie, CIC1401, Proteomics Facility, Pessac, France. [2]INSERM, Centre de Recherche Cardio-thoracique de Bordeaux, U1045, CIC1401, Pessac, France. [3]Univ-Lorraine, Institut Elie Cartan de Lorraine, UMR7502, Vandoeuvre-lès-Nancy, France. [4]Helmholtz Institute for RNA-based Infection Research (HIRI), Helmholtz-Center for Infection Research (HZI), Würzburg, Germany. [5]CHU de Bordeaux, Service d'exploration fonctionnelle respiratoire, CIC1401, Pessac, France. [6]Univ. Bordeaux, CNRS, Interdisciplinary Institute for Neuroscience, IINS, UMR 5297, Bordeaux, France. [7]Univ. Bordeaux, CNRS, INSERM, Bordeaux Imaging Center, BIC, UAR3420, US 4, Bordeaux, France. [8]CNRS, UMR5164 ImmunoConcEpT, Université de Bordeaux, Bordeaux, France. [9]CHU de Bordeaux, Laboratoire d'Immunologie et Immunogénétique, Bordeaux, France

*** Corresponding author:** Pr Isabelle DUPIN, PhD
Centre de recherche Cardio-thoracique de Bordeaux INSERM U1045
PTIB - Hôpital Xavier Arnozan, Avenue du Haut Lévêque, 33600 PESSAC
e-mail: isabelle.dupin@u-bordeaux.fr

Abstract

Bronchi of chronic obstructive pulmonary disease (COPD) are the site of extensive cell infiltration, allowing persistent contacts between resident cells and immune cells. Tissue fibrocytes interaction with $CD8^+$ T cells and its consequences were investigated using a combination of *in situ*, *in vitro* experiments and mathematical modeling. We show that fibrocytes and $CD8^+$ T cells are found in vicinity in distal airways and that potential interactions are more frequent in tissues from COPD patients compared to those of control subjects. Increased proximity and clusterization between $CD8^+$ T cells and fibrocytes are associated with altered lung function. Tissular $CD8^+$ T cells from COPD patients promote fibrocyte chemotaxis via the CXCL8-CXCR1/2 axis. Live imaging shows that $CD8^+$ T cells establish short-term interactions with fibrocytes, that trigger $CD8^+$ T cell proliferation in a CD54- and CD86-dependent manner, pro-inflammatory cytokines production, $CD8^+$ T cell cytotoxic activity against bronchial epithelial cells and fibrocyte immunomodulatory properties. We defined a computational model describing these intercellular interactions and calibrated the parameters based on our experimental measurements. We show the model's ability to reproduce histological ex vivo characteristics, and observe an important contribution of fibrocyte-mediated $CD8^+$ T cell proliferation in COPD development. Using the model to test therapeutic scenarios, we predict a recovery time of several years, and the failure of targeting chemotaxis or interacting processes. Altogether, our study reveals that local interactions between fibrocytes and $CD8^+$ T cells could jeopardize the balance between protective immunity and chronic inflammation in bronchi of COPD patients.

Introduction

The prevalence of COPD, one of the most common chronic diseases worldwide, has been rising in recent decades (Mannino & Buist, 2007); thus, prevention and treatment of COPD are important issues of global healthcare. COPD bronchi are an area of intense immunological activity and tissue remodeling, as evidenced by the extensive immune cell infiltration and changes in tissue structures such as peribronchial fibrosis. In particular, distal airways are hypothesized to constitute a "quiet zone", where exaggerated remodeling and inflammatory processes take place early in the history of the disease, without identifiable symptoms or lung function tests alteration (Hogg et al., 1970; Mead, 1970). In these particular areas, persistent contacts occur between resident cells and stimulated immune cells migrating from the peripheral circulation to the distal airways. The relevance of direct contact between T cells and monocyte-macrophages to potentiate the inflammatory response has been demonstrated in many chronic inflammatory diseases affecting the central nervous system, osteoarticular structures and the lungs (Dayer, 2003), but remains to be fully investigated in COPD.

Fibrocytes, fibroblast-like leukocytes, produced by the bone marrow and released in the peripheral circulation (R. Bucala et al., 1994), have been implicated in lung fibrosis (Pilling et al., 2014). They are also recruited in the blood of COPD patients during an acute exacerbation (Dupin et al., 2016). High circulating fibrocyte count during a COPD exacerbation is associated with an increased risk of death, suggesting that fibrocytes could be detrimental to the evolution of this disease (Dupin et al., 2016). We have also demonstrated that tissue fibrocytes density increases in COPD bronchi, which was associated with a degraded lung function, increased wall thickness and air trapping (Dupin et al., 2019). However, the function of these fibrocytes in COPD lungs is not yet fully understood (Dupin et al., 2018). Besides their role in tissue scarring matrix production (R.

Bucala et al., 1994) and contraction (Henrot et al., 2022), recruited fibrocytes may participate to lung inflammation in virtue of their immune properties. They can function as antigen-presenting cells with T cells (Chesney et al., 1997), which can in turn modulate fibrocyte differentiation (Abe et al., 2001; Niedermeier et al., 2009). Fibrocyte engagement into immunomodulation has been implicated in various diseases such as thyroid-associated ophthalmopathy (Fernando et al., 2012) and lung cancer (Afroj et al., 2021). Cytotoxic $CD8^+$ T cells are predominant in the airways of COPD patients and their number inversely correlates with lung function (O'Shaughnessy et al., 1997). $CD8^+$ T cell-deficient mice are protected against lung inflammation and emphysema induced by cigarette smoke exposure (Maeno et al., 2007) whereas the expression of molecules linked to tissue destruction, such as perforin, granzyme B and ADAM15, correlate with disease severity (Freeman et al., 2010; Wang et al., 2020), suggesting $CD8^+$ T cells implication in lung inflammation and destruction in COPD. Activation of $CD8^+$ T cells is increased in COPD lung samples (Roos-Engstrand et al., 2009). Other studies have shown that $CD8^+$ T cell activation could be partially T Cell Receptor (TCR)-independent (Freeman et al., 2010). The absence of increased expression of cytotoxic enzyme in peripheral blood $CD8^+$ T cells from COPD patients argues in favor of a local activation within the lungs (Morissette et al., 2007). $CD8^+$ T cells express an exhausted phenotype in the COPD lung, that may result from an over-activation thus participating to the defective response to infection in COPD (McKendry et al., 2016). However, $CD8^+$ T cells activation's mechanism as well as their precise contribution to COPD pathogenesis remain largely unknown.

A recent study showed that fibrocytes, derived from the blood of lung adenocarcinoma patients, could strongly enhance the proliferation of $CD8^+$ T cells (Afroj et al., 2021). We thus hypothesized that $CD8^+$ T cells and fibrocytes interact into the lungs, and that this interaction is critical in COPD pathology. Multiple immunostainings in combination with

specific image analysis methods allow to determine the spatial distribution of individual $CD8^+$ T cells and fibrocytes within bronchial tissues of both control subjects and COPD patients. Using *in vitro* fibrocyte and $CD8^+$ T cell–based experiments, we studied cell interplay in terms of relative chemotaxis, dynamics, proliferation and cytokine secretion profile. We then integrated these findings into an agent-based computational model representing airways from either healthy or COPD patients enabling to test how local interactions shape spatial distributions of cell in both conditions. We propose that slight dysregulations of intercellular interactions induce abnormal cell organization around bronchi, ultimately causing a breakdown of tissue homeostasis, leading to chronic inflammation and tissue remodeling.

Results

Direct contacts between fibrocytes and CD8$^+$ T cells are more frequent in distal bronchial tissue from COPD patients than in that of controls

We used immunohistochemistry (IHC) to assess whether fibrocytes and CD8$^+$ T cells were in close vicinity in human tissue. Sections of distal lung tissues from 17 COPD and 25 control patients were obtained, from a previously described cohort (Dupin et al., 2019), and labeled to detect CD8$^+$ T cells, identified as cells positive for CD8 staining and fibrocytes, identified as cells dual positive for FSP1 and CD45 double staining (Figure S1A-D). In agreement with previous studies (Dupin et al., 2019; O'Shaughnessy et al., 1997; Saetta et al., 1998), the density of both CD8$^+$ T cells and fibrocytes was increased within the subepithelial area of distal bronchi from COPD patients compared with that of control subjects (Figure 1A-C). Moreover, fibrocytes and CD8$^+$ T cells were frequently in close proximity (Figure 1D). To quantify the potential for cell–cell contacts, we determined the density of CD8$^+$ T cells in interaction with CD45$^+$ FSP1$^+$ cells (Figure S1A-D). Whatever the magnification used to automatically count interacting cells, the density of CD8$^+$ T cells in interaction with fibrocytes was higher in the sub-epithelial region of distal bronchi of COPD patients than in that of control subjects (Figure 1D-F). For subsequent analyses, we chose the dilatation size "D8" (3.6 µm, which represents the radius of a mean ideal round cell in our analysis) to reflect the density of interacting cells. To evaluate the minimal distance between CD45$^+$ FSP1$^+$ cells and neighboring CD8$^+$ T cells, we used a CD8 distance map generated from the CD8 staining image, with the brightness of each pixel reflecting the distance from a CD8$^+$ T cell (Figure S1E-F). The mean minimal distance between fibrocytes and CD8$^+$ cells was significantly smaller in the sub-epithelial region of distal bronchi of COPD patients than in that of control subjects (Figure 1G-H). In contrast, the mean minimal distances between CD8$^+$ T cells themselves or between fibrocytes themselves were

unchanged (Figure S2A-B). The majority of both $CD8^+$ T cells and fibrocytes was located beneath the epithelium, with their minimal distance and distribution relatively to the basal membrane being similar in control and COPD patients (Figure S2C-F). Altogether, no difference of spatial repartition was observed within each cell population between control and COPD patients, but the relative distribution of fibrocytes and $CD8^+$ cells was affected in tissues from patients with COPD.

To further describe the relative spatial organization of both cell types, we used a method based on Delaunay triangulation computed on previously segmented cell barycenters. It is based on a custom developed plugin to determine congregations of small groups of cells, called "clusters" (Figure S3). As expected from our minimal distance analysis, we found difference neither in the density of single cell-type clusters nor in their size, measured by the mean number of cells by cluster, between control subjects and patients with COPD (Figure 1I-J, left and middle panels). However, the density of clusters containing both cell types ("mixed cell clusters") was higher in distal bronchi of COPD patients than in those of control subjects, with a median number of 5 and 6 cells in these clusters in control and COPD tissues, respectively (Figure 1I-J, right panels). This result indicates that fibrocytes and $CD8^+$ T cells are found within close proximity in the peribronchial area of COPD patients, with possible co-organization of $CD8^+$ T cells and fibrocytes in mixed cell clusters, indicating that direct and/or indirect fibrocyte-$CD8^+$ T cell interactions might occur *in vivo*.

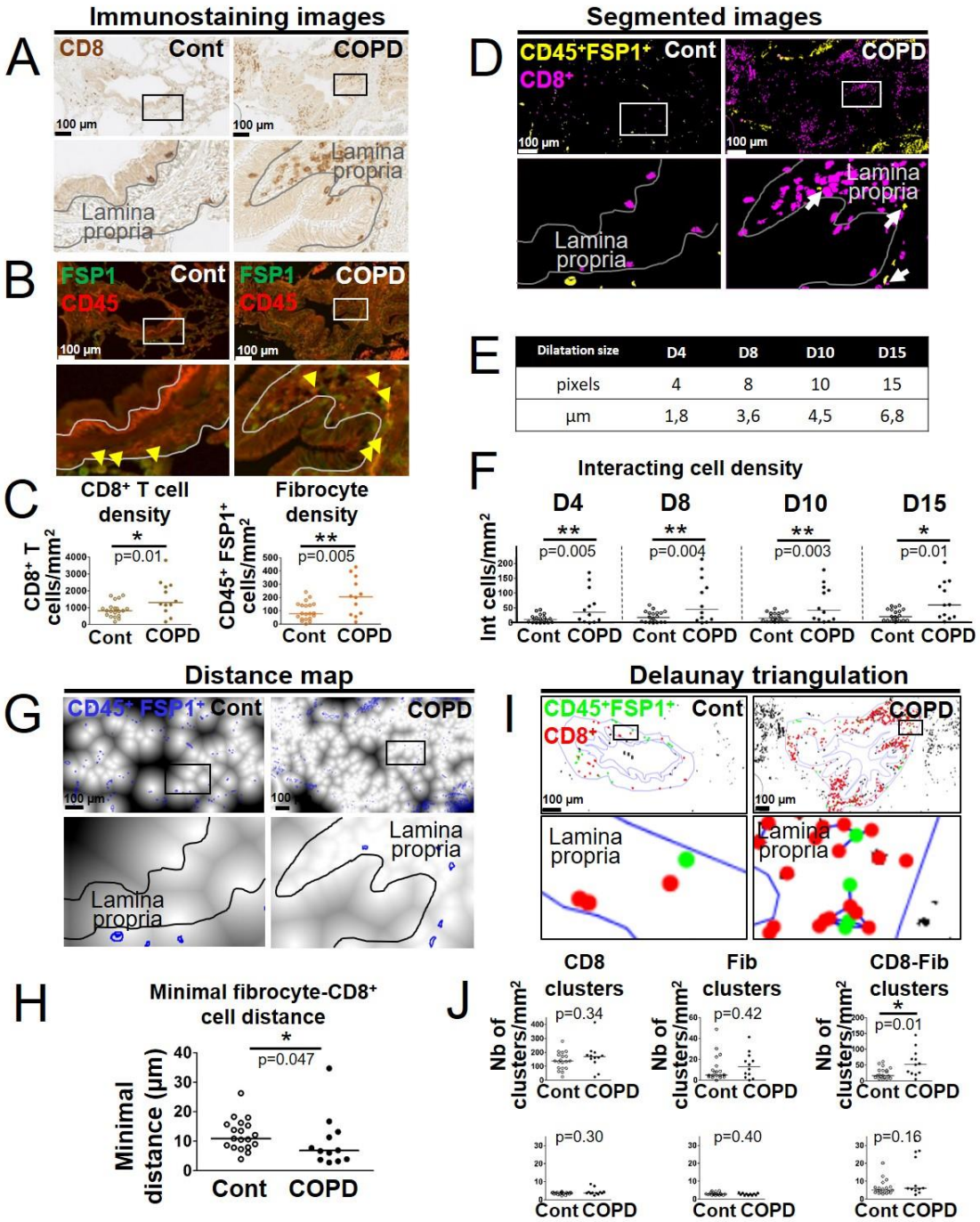

Figure 1. Increased interactions between CD8$^+$ T cells, CD45$^+$ FSP1$^+$ cells in distal airways of COPD patients. (A, **B**) Representative stainings of CD8 (brown, **A**), CD45 (red, **B**) and FSP1 (green, **B**) in distal bronchial tissue specimens from a control subject (left) and a COPD patient (right). The yellow arrowheads indicate fibrocytes, defined as CD45$^+$ FSP1$^+$ cells. (**C**) Quantification of CD8$^+$ T cells and fibrocyte densities (normalized by the sub-epithelial area) in one specimen/patient (n=20 control subjects, n=12 patients with COPD). (**D**) Merged segmented images for CD8 and CD45-FSP1 staining, showing CD8$^+$ T cells and CD45$^+$ FSP1$^+$ cells respectively in magenta and yellow. The white arrows indicate interacting cells, detected by dilatation of CD8 positive particle. (**E**) Table showing the correspondence between dilatations in pixels and µm. F, Quantification of interacting cells densities (normalized by the sub-epithelial area) in one specimen/patient, using the different dilatations sizes (**E**). (**G**) Distance maps built from the binary image produced from CD8

staining, with FSP1$^+$ CD45$^+$ cells (blue outlines). (**H**) Quantification of the mean minimal distances between fibrocyte and CD8$^+$ T cells in one specimen/patient. (**I**) Cluster analysis performed by Delaunay triangulation on segmented images for CD8 and CD45-FSP1 staining, followed by the application of a threshold value (40 µm) above which connections are not kept. CD8$^+$ T cells and fibrocytes appear respectively with green and red dots, connections are shown in blue. (**J**) First row: densities of clusters containing exclusively CD8$^+$ T cells ("CD8 clusters"), fibrocytes ("Fib clusters") and both cell types ("CD8-Fib clusters") normalized by the sub-epithelial area) in one specimen/patient. Second row: mean number of cells by cluster. (**C, F, H, J**) The medians are represented as horizontal lines, n=20 specimens from control subjects, n=12 specimens from patients with COPD. *: P<0.05, **:P<0.01; ***: P<0.001. unpaired t-tests or Mann Whitney tests.

Relationships between the density of CD8$^+$ T cells interacting with fibrocytes and functional parameters

We determined the univariate correlation coefficients between fibrocyte density, CD8$^+$ T cell density, the 3 variables quantifying the interaction of CD8$^+$ T cells with fibrocytes (the interacting cell density, the mean minimal distance between fibrocytes and CD8$^+$ T cells and the density of mixed cell clusters), and various functional and CT parameters (Tables S1 to S5). In particular, moderate but significant univariate correlations were found between the Forced Expiratory Volume in 1 second / Forced Vital Capacity (FEV_1/FVC) ratio (used to diagnose COPD if below 0.7) and the density of fibrocytes, the density of interacting cells, the mean minimal distance between fibrocytes and CD8$^+$ T cells and the density of fibrocytes-CD8$^+$ T cells clusters (Figure S4A-D). Variables significantly correlated with FEV_1/FVC were entered into stepwise regression analyses in order to find the best model fitting FEV_1/FVC. The best model associated the density of interacting cells and the density of mixed cell clusters. It explained 35% of the FEV_1/FVC variability (Table S6). The relationships between the FEV_1/FVC ratio, the density of interacting cells and the density of mixed cell clusters were all statistically significant.

Chemo-attraction of CD8$^+$ T cells for fibrocytes is increased in COPD tissue

To decipher the molecular mechanisms underpinning the increased cell-cell interaction in COPD bronchi, we investigated cell adhesion and chemotaxis processes in $CD8^+$ T cells of patients with COPD compared with those of controls. Using the transcriptomic profile of tissular resident memory and effector memory $CD8^+$ T cells of COPD patients compared with that of control subjects in the GSE61397 microarray dataset (http://www.ncbi.nlm.nih.gov/geo/) published elsewhere (Hombrink et al., 2016), we noted significative changes in the abundance of transcripts of genes related to cell adhesion. However, the changes were not consistent with clear increased or decreased adhesive properties in both tissue resident memory $CD8^+$ $CD103^+$ T-cells (T_{RM}) and effector memory $CD8^+$ $CD103^-$ T-cells (T_{EM}) (Figure S5). In contrast, transcriptomic data reveal consistent changes in COPD cells *versus* controls, mostly increases, in chemokines and chemokine receptors (Figure 2A). Most changes in transcripts were compatible with a pro-attractive and a pro-migratory response. In particular, there were increases of CCL2, CCL26, CXCL2 and CXCL8 expression in T_{RM} from patients with COPD, and CCL3L1 expression in T_{EM} from patients with COPD (Figure 2A).

We then investigated whether tissular $CD8^+$ T cells secretion from control or COPD patients could affect fibrocytes migration in an *in vitro* assay (Figure 2B). $CD8^+$ T cells were purified from lung resection material sampled either in control subjects or in COPD patients, whose characteristics are reported (Table S7). Precursors of fibrocytes were purified from blood samples of a separate cohort of COPD patients (*i.e.*, COBRA), whose characteristics are also reported (Table S8). The migration of fibrocytes was significantly increased by conditioned medium derived from tissular $CD8^+$ T cells of COPD patients compared with those from control lungs (Figure 2C).

The secretory profile of these tissular $CD8^+$ T cells 36h after culture conditions with soluble anti-CD3 and anti-CD28 antibodies was determined. The concentration of CXCL8 was

increased in $CD8^+$ T cells from COPD patients compared to control cells (Figure 2D) in good agreement with the transcriptomic analysis. By contrast, the concentration of both CCL3 and CCL3L1 was undetectable (data not shown), whereas that of CCL2, CXCL1, CXCL2, CXCL3, CXCL5 and CXCL6 remained unchanged (Figure 2D). Since CXCL8 is a ligand of the chemokine receptors CXCR1 and/or CXCR2, we repeated the migration assay with the addition of the drug reparixin, an antagonist of both CXCR1 and CXCR2 (Bertini et al., 2004). Whereas fibrocyte treatment with reparixin had no significant effect on the control $CD8^+$ T cells-mediated migration, it did inhibit the increased migration induced by the secretions of $CD8^+$ T cells purified from COPD tissues (Figure 2E). Moreover, an anti-CXCL8 blocking antibody also inhibited the increased migration induced by the secretions of $CD8^+$ T cells purified from COPD tissues, in the same extend than the blocking of CXCR1/2 by reparixin (Figure 2F), suggesting that this supplementary chemotaxis is mainly due to CXCL8 and not other CXCR1/2 binding CXCL chemokines. These data indicate that tissular $CD8^+$ T cells from patients with COPD promote fibrocyte chemotaxis via CXCL8-CXCR1/2 axis.

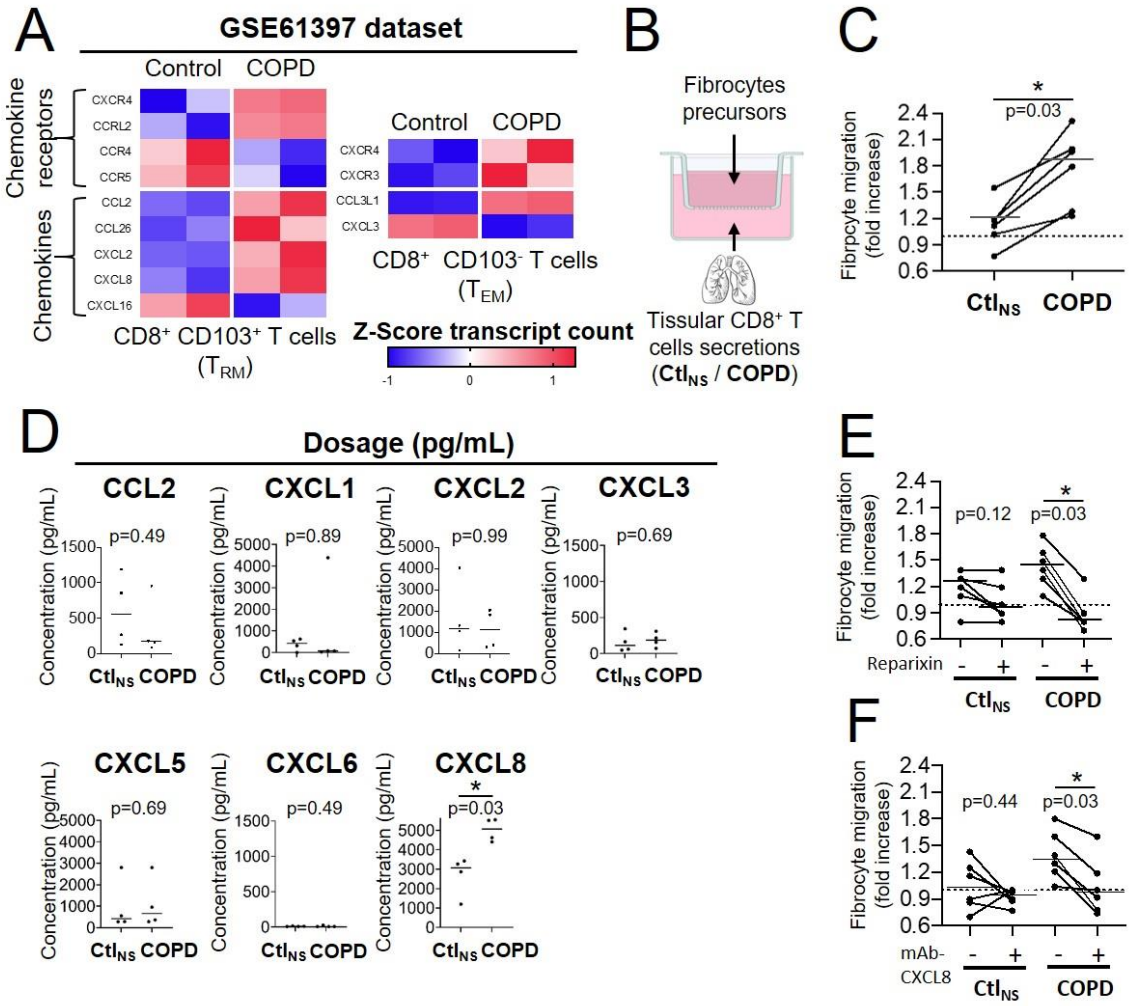

Figure 2. CD8⁺ T cells from COPD tissue have increased chemoattractive properties for fibrocytes. (A) Heatmaps showing the expression of differentially expressed genes with p-value<0.05 of chemokines and chemokine receptors in resting tissular tissue resident memory T-cells (T_{RM}) and effector memory T-cells (T_{EM}) from patients with COPD (n=2 independent samples) in comparison with control subjects (n=2 independent samples) (GEO accession GSE61397). Expression values are expressed as Z-score transformed transcript count. (**B**) Migration experiment design. (**C**) Migration of fibrocytes from patients with COPD in response to $CD8^+$ T cells supernatants from control subjects (Ctl_{NS}) or COPD patients (COPD). n=6 independent experiments (**D**) CCL2, CXCL2 and CXCL8 levels in $CD8^+$ T cells supernatants from non-smoking control subjects (Ctl_{NS}) or patients with COPD (COPD) using BioPlex (CCL2, CXCL2) or ELISA (CXCL1, 3, 5, 6, 8). n=4 Ctl_{NS} samples, n=4 COPD samples. * $P < 0.05$, Mann–Whitney test. (**E-F**), Migration of fibrocytes from patients with COPD in response to $CD8^+$ T cells supernatants from control subjects (Ctl_{NS}) or COPD patients (COPD), in the presence of 200nM Reparixin (+) or corresponding vehicle (-) (**E**), and in the presence of 1µg/mL blocking antibody for CXCL8 (+) or control antibody (-) (**F**). n=6 independent experiments * $P < 0.05$, Wilcoxon matched pairs test.

CD8$^+$ T cells repeatedly interact with fibrocytes

As fibrocytes and CD8$^+$ T cells reside in close proximity in the subepithelial area, especially that of tissues from COPD patients, we investigated their crosstalk capacity. We developed an autologous *in vitro* co-culture system allowing precise control over the cell types involved. Fibrocytes and CD8$^+$ T cells, both purified from blood of COPD patients were co-cultured 2 days before image acquisition for the following 12h. CD8$^+$ T cells were either nonactivated or activated with anti-CD3/CD28 antibodies coated microbeads, whereas fibrocytes were not stimulated. At the beginning of live imaging, nonactivated CD8$^+$ T cells were equally allocated in fibrocyte-covered zones (41 ± 8%) and in fibrocyte-free zones (59% ± 8%) (Figure 3A-B). Twelve h later, most (77 ± 9%) of CD8$^+$ T cells were present in contact with fibrocytes (Figure 3A-B). Activation of CD8$^+$ T cells resulted in similar distribution (Figure 3A-B). These data suggest that both cell types are able to directly interact, and that these interactions progressively increase during co-culture. We tracked individual CD8$^+$ T cells during 12h time lapse to capture their spatiotemporal dynamics using multiple variables quantification (Figure 3C and Movie S1). For both nonactivated and activated lymphocytes, the mean speed of CD8$^+$ T cells decreased upon contact with fibrocytes (Figure 3D). Irrespective of the activation state of CD8$^+$ T cells, a majority of intercellular contacts (49 ± 6% and 49 ± 8% for nonactivated and activated CD8$^+$ T cells, respectively) were short-lived (<12 min) and dynamic, although some longer interactions (>32 min) could also be detected (30 ± 4% and 27 ± 7% for nonactivated and activated CD8$^+$ T cells, respectively) (Figure 3E). The contact coefficient and the mean velocity of CD8$^+$ T cells measured in the absence of contact with fibrocytes ("Mean free speed") were similar in both conditions of activation (Figure 3F-G). However, we observed a significant decrease in the mean speed for activated CD8$^+$ T cells when they were in contact with

fibrocytes ("Mean contact speed") compared to nonactivated CD8$^+$ T cells (Figure 3H), reflecting subtle behavior changes in this condition of activation.

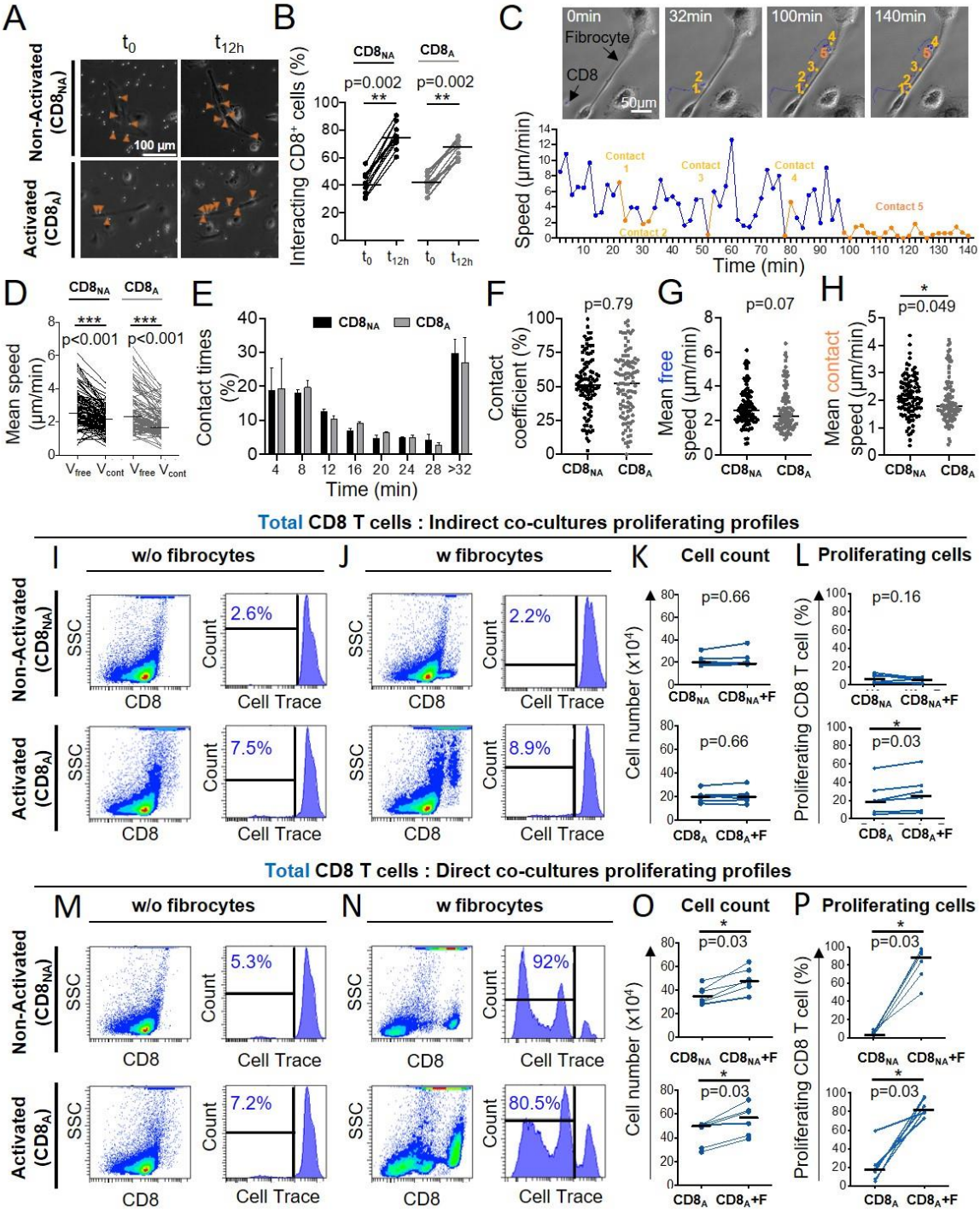

Figure 3. CD8$^+$ T cell repeatedly contact fibrocytes and this contact greatly enhances CD8$^+$ T cell proliferation. Prior to co-culture, CD8$^+$ T cells have been either non-activated ("CD8$_{NA}$") or activated ("CD8$_A$"). (**A**) Representative brightfield images of co-culture between CD8$^+$ T cells and fibrocytes at the initial state of the acquisition (t_0) and after 12 hours (t_{12h}) in both conditions of activation. The orange arrowheads indicate CD8$^+$ T cells (bright round-shaped cells) in contact with fibrocytes (elongated adherent cells). (**B**)

Quantifications of the proportion of fibrocyte-interacting $CD8^+$ T cells at t_0 and t_{12h} in both conditions of activation. (**C**) Top panel: typical $CD8^+$ T cells trajectory (blue) relatively to a fibrocyte (elongated adherent cell) for a period of 140 min. Bottom panel: speed (µm/min) over time for the tracked $CD8^+$ T cell. Short-lived (<12 min, n=4) and longer-lived (>32 min, n=1) contacts are represented respectively in light and dark orange. (**D**) Comparison of the mean speed of individual $CD8^+$ T cells measured in the absence ("V_{free}") or presence ("V_{cont}") of contact with fibrocytes in both conditions of activation. (**E**) Mean frequency distributions of contact time duration (with 4 min binning) between $CD8^+$ T cells and fibrocytes for $CD8_{NA}$ (black) and $CD8_A$ (gray). Error bars indicate standard error of the mean. Two-way ANOVA (**F-H**) Dot plots representing spatiotemporal variables measured for each individual $CD8^+$ T cell tracked over 12h. Each dot represents one cell. (**F**) Contact coefficient. (**G**) Mean speed of $CD8^+$ T cells measured in the absence of contact with fibrocytes ("Mean free speed"). (**H**) Mean speed of $CD8^+$ T cells measured in the presence of contact with fibrocytes ("Mean contact speed"). (**A-H**) n=2 independent experiments, n=10 movies by experiments, n=10 $CD8^+$T cells tracked by movies. (**I, J, M, N**) Representative gating strategy for identification of $CD8^+$ T cells without (w/o) fibrocytes (**I, M**) or with (w) fibrocytes (**J, N**) in indirect (**I, J**) or direct (**M, N**) co-culture. Left panels: dot plots represent representative CD8-PerCP-Cy5-5 fluorescence (y-axis) versus side scatter (SSC, x-axis) of non-adherent cells removed from the culture. Right panels: histograms represent representative cell count (y-axis) versus Cell Trace-Pacific Blue fluorescence (x-axis). The distinct fluorescence peaks correspond to the different generations of $CD8^+$ T cells. The gate and the percentage indicate cells that have proliferated. (**K**, **O**) Comparison of manual count of non-adherent cells removed from co-culture without fibrocyte ("CD8") and with fibrocyte ("CD8+F"). L, (**P**) Comparison of quantifications of $CD8^+$ T cells that have proliferated, removed from co-culture without fibrocyte ("CD8") and with fibrocyte ("CD8+F"). (**I-P**) n=6 independent experiments. (**B**, **D**, **F**, **G**, **H**, **K**, **L**, **O**, **P**) Medians are represented as horizontal lines. * $P < 0.05$, ** $P < 0.01$, *** $P < 0.001$. (**B**, **D**, **K**, **L**, **O**, **P**) Wilcoxon matched pairs test. (**F**, **G**, **H**) Mann Whitney tests.

Fibrocytes favor $CD8^+$ T cell proliferation in a cell-cell contact-dependent manner

Since multiple transient contacts have been shown to be an early trigger of events leading to clonal expansion (Obst, 2015), we wondered whether fibrocytes could promote $CD8^+$ T cells proliferation using total cell count and a CellTrace-based co-culture proliferation assay. We designed two different co-culture assays modeling either a direct contact between the two cell types or an indirect contact (transwell assay). The activation of $CD8^+$ T cells by anti-CD3/CD28 antibody coated microbeads slightly increased the basal level of dividing $CD8^+$ T cells (comparison of the conditions "$CD8_{NA}$" and "$CD8_A$" without fibrocytes in Figure 3I-P). The presence of fibrocytes in the indirect co-culture assay did not affect proliferation capacity of non-activated $CD8^+$ T cells and only moderately increased the

number of dividing activated $CD8^+$ T cells (Figure 3 I-L). The distinction between naïve ($CD45RA^+$) and memory ($CD45RA^-$) $CD8^+$ T cells did not reveal any selective effect of fibrocytes on these two $CD8^+$ subpopulations (Figure S6A, C and S6E-H). In the direct co-culture model, the total number of $CD8^+$ T cells and the percentage of dividing $CD8^+$ T cells were far higher in the presence of fibrocytes irrespective of the activation state of $CD8^+$ T cells (Figure 3M-P). This effect seemed to be particularly impressive for naïve $CD8^+$ T cells as they demonstrated an average differential of 80 ± 14% and 70 ± 20% of dividing cells between the conditions with and without fibrocytes, respectively for nonactivated (Figure S6I-J, top panels) and activated $CD8^+$ T cells (Figure S6I-J, bottom panels), *vs* 67 ± 18% and 52 ± 20% for memory $CD8^+$ T cells (Figure S6K-L). We also performed co-cultures between fibrocytes and $CD4^+$ T cells, with the same settings than for $CD8^+$ T cells. The results from these experiments show that fibrocytes did not have any significant effect of $CD4^+$ T cells death, irrespective of their activation state (Figure S7A-C). Fibrocytes were able to promote $CD4^+$ T cells proliferation in the activated condition but not in the non-activated condition (Figure S7A-D). Altogether, this implies that a direct rather than indirect interactions between $CD8^+$ T cells and fibrocytes increased $CD8^+$ T cell proliferation, and that although fibrocyte-mediated effect on proliferation is not specific to $CD8^+$ T cells, the extend of the effect is much larger on $CD8^+$ T cells than on $CD4^+$ T cells.

Taking advantage of the staining of $CD8^+$ T cells with the death marker Zombie NIR™, we have also quantified $CD8^+$ T cell death in our co-culture assay. The presence of fibrocytes in the indirect co-culture assay did not affect $CD8^+$ T cell death (Figure S8A-B). In direct co-culture, the death of $CD8^+$ T cells was significantly increased in the non-activated condition but not in the activated condition (Figure S8C-D).

After 6 days of co-culture, a cell population with a low level of CD8 expression ($CD8^{low}$) appeared, that was inversely proportional to the level of $CD8^+$ T cells strongly expressing a

high level of CD8 ($CD8^{high}$, Figure S9). The CellTrace-based assay showed that those cells highly proliferated during co-culture, especially in the direct co-culture (Figure S9E), suggesting that $CD8^{high}$ cells disappeared in favor of $CD8^{low}$ cells. As fibrocytes could have contaminated the cell suspension harvested from the direct co-culture, we did check that those $CD8^{low}$ cells were not $CD45^{+}$ Collagen I^{+} (Figure S10). Phenotypic analysis of this $CD8^{low}$ population indicated that cells were mostly $CD45RA^{-}$ cells (Figure S9A-B, S9D-E), with a low level of cytokine expression (Figure S9C, F). Since $CD8^{low}$ cells may thus represent a population of exhausted T cells, we focused on $CD8^{high}$ cells in the following, especially regarding the secretion profile characterization. As CD86 and CD54 co-stimulatory molecule and adhesion molecule, respectively, pivotal in immunological synapse formation, are both expressed by fibrocytes (Afroj et al., 2021; Balmelli et al., 2005), we tested the effects of anti-CD54 and anti-CD86 blocking antibodies on fibrocyte-induced proliferation of $CD8^{+}$ T cells. The inhibition of CD86 and CD54 significantly reduced proliferation of nonactivated $CD8^{+}$ T cells in the direct co-culture with fibrocytes (Figure 4). However, these antibodies failed to alter the stimulatory activity of lymphocyte division by fibrocytes, when $CD8^{+}$ T cells were previously activated (Figure 4). Blocking LFA-1 did not affect the fibrocyte-mediated $CD8^{+}$ T cell division (Figure S11A-D), suggesting the existence of compensatory integrins at the surface of the lymphocyte, such as CD11b/CD18, to mediate the interaction with CD54. The inhibition of CD44, a receptor for hyaluronan which has been shown to be produced by fibrocytes (Bianchetti et al., 2012), did not impair the proliferation of $CD8^{+}$ T cells irrespective of their activation state (Figure S11E-H).

In total, these results indicate that direct contacts between fibrocytes and $CD8^{+}$ T cells, such as those mediated by CD54 and CD86, were strong positive signals to trigger $CD8^{+}$ T cell proliferation with the induction of $CD8^{high}$ and $CD8^{low}$ phenotypes.

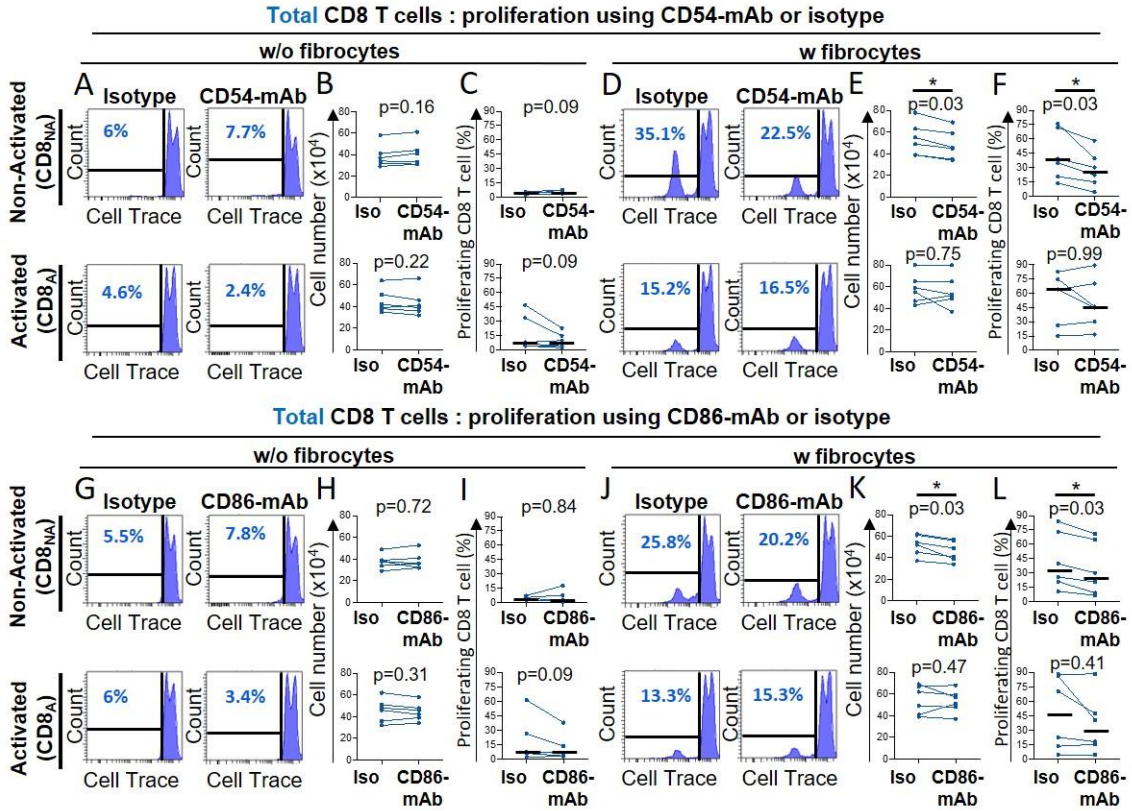

Figure 4. Fibrocytes act as a major promoter on CD8$^+$ T cell proliferation in a CD54 and CD86-dependent manner. Prior to co-culture, CD8$^+$ T cells have been either non-activated ("CD8$_{NA}$") or activated ("CD8$_A$"). (**A**, **D**, **G**, **J**) Representative gating strategy for identification of proliferating CD8$^+$ T cells without (w/o) fibrocytes (**A**, **G**) or with (w) fibrocytes (**D**, **J**) using neutralizing CD54-mAb (**A**, **D**) or neutralizing CD86-mAb (**G**, **J**) and respective control isotype. Histograms represent representative cell count (y-axis) versus Cell Trace-Pacific Blue fluorescence (x-axis). The distinct fluorescence peaks correspond to the different generations of CD8$^+$ T cells. The gate and the percentage indicate cells that have proliferated. (**B**, **E**, **H**, **K**) Comparison of manual count of non-adherent cells removed from co-culture treated with neutralizing CD54-mAb or control isotype (Iso) (**B**, **E**) and neutralizing CD86-mAb or control isotype (Iso) (**H**, **K**). (**C**, **F**, **I**, **L**) Comparison of quantifications of CD8$^+$ T cells that have proliferated, removed from co-culture treated with neutralizing CD54-mAb (**C**, **F**) or neutralizing CD86-mAb (**I**, **L**) and respective control isotype. n=6 independent experiments. Medians are represented as horizontal lines. * $P < 0.05$, Wilcoxon matched paired tests.

Fibrocyte-CD8$^+$ T cell interactions alter cytokine production and promotes CD8$^+$ T cell cytotoxicity

Multiparametric flow cytometry was used to characterize the cytokine expression profile of CD8$^+$ T cells in the indirect and direct co-culture with fibrocytes. When nonactivated CD8$^+$ T cells were indirect co-cultured with fibrocytes, the expression of TNF-α, IFN-γ by CD8$^+$

T cells was slightly increased (Figure 5A-B). IL-10, IL-17 and Granzyme B were not detected (Figure 5A-B). When $CD8^+$ T cells were activated with anti-CD3/CD28, the level of TNF-α and IFN-γ further increased, and the expression of granzyme B and IL-10 was slightly induced (Figure 5A-B). Upon direct co-culture, we observed a massive induction of TNF-α, IFN-γ, granzyme B, IL-10 and IL-17, irrespective of the activation state of $CD8^+$ T cells (Figure 5C-D). Altogether, these results show that soluble factors and direct contacts between fibrocytes and $CD8^+$ T cells might have an additive effect on $CD8^+$ T cell cytokine production. The concentration of TNF-α measured in culture supernatant increased significantly upon co-culture between fibrocytes and non-activated $CD8^+$ T cells at day 4, confirming that TNF-α was secreted in the medium upon direct interactions with fibrocytes (Figure 5E). This shows that both soluble factors produced by fibrocytes and direct contacts influence $CD8^+$ T cell secretion profile.

We then wondered whether glucocorticoid drugs (*i.e.*, budesonide or fluticasone propionate) could reverse the fibrocyte-induced proliferation and differentiation of $CD8^+$ T cells. Treatment with glucocorticoid drugs significantly decreased fibrocyte-induced TNF-α secretion by non-activated $CD8^+$ T cells, without affecting the proliferation (Figure S12). Collectively, these results underline the importance of the interaction with fibrocytes for $CD8^+$ T cell activation, possibly by favoring cellular proliferation and local cytokine production.

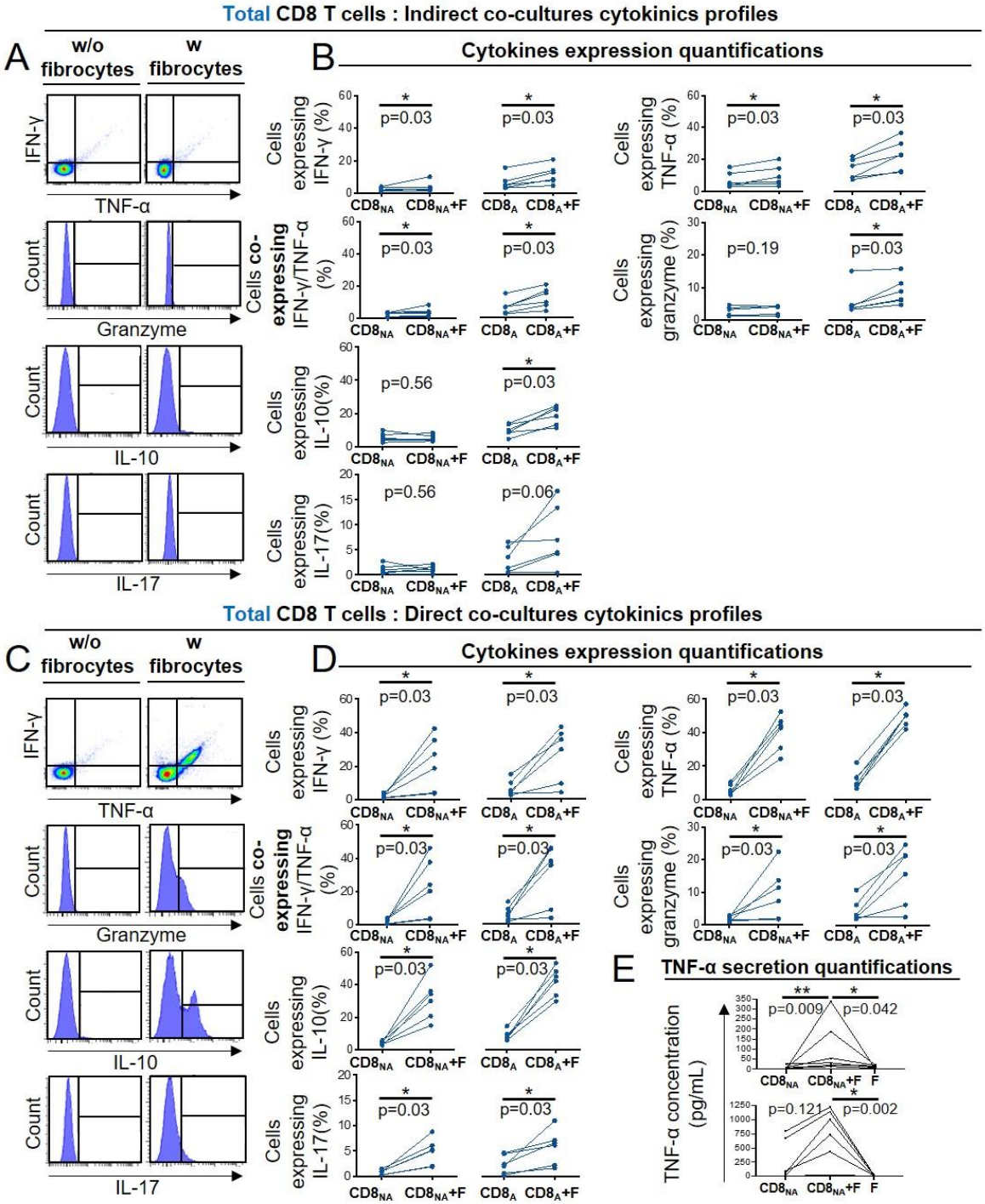

Figure 5. Fibrocyte-CD8$^+$ T cell interactions alter cytokine production. Prior to co-culture, CD8$^+$ T cells have been either non-activated ("$CD8_{NA}$") or activated ("$CD8_A$"). (**A**, **C**) Representative gating strategy for identification of CD8$^+$ T cells expressing IFN- γ, TNF-α, granzyme, IL-10 and IL17 without (w/o) fibrocytes (left panel) or with (w) fibrocytes (right panel) in indirect (**A**) or direct (**C**) co-culture. (**B**, **D**) Quantifications of CD8$^+$ T cells expressing IFN-γ, TNF- α, both, granzyme and IL-10 after co-culture without fibrocytes ($CD8_{NA}$/$CD8_A$) or with fibrocytes ($CD8_{NA}$/$CD8_A$ +F) in indirect (**B**) or direct (**D**) co-culture. (**E**) TNF-α concentrations in supernatants from co-cultures without fibrocytes ($CD8_{NA}$/$CD8_A$), with fibrocyte ($CD8_{NA}$/$CD8_A$ +F), and only with fibrocytes (F) as control, for direct co-cultures. n=6 independent experiments. * $P < 0.05$, Wilcoxon matched paired tests or Friedman tests.

Having shown that fibrocytes promoted CD8$^+$ T cells expression of cytotoxic molecules such as granzyme B, we decided to investigate the cytotoxic capacity of CD8$^+$ T cells against primary basal bronchial epithelial cells (see Table S9 for patient characteristics). Direct co-culture with fibrocytes increased total and membrane expression of the cytotoxic degranulation marker CD107a, which was only significant in non-activated CD8$^+$ T cells (Figure 6A-E). A parallel increase of cytotoxicity against primary epithelial cells was observed in the same condition (Figure 6F-H). This demonstrates that following direct interaction with fibrocytes, CD8$^+$ T cells have the ability to kill target cells such as bronchial epithelial cells.

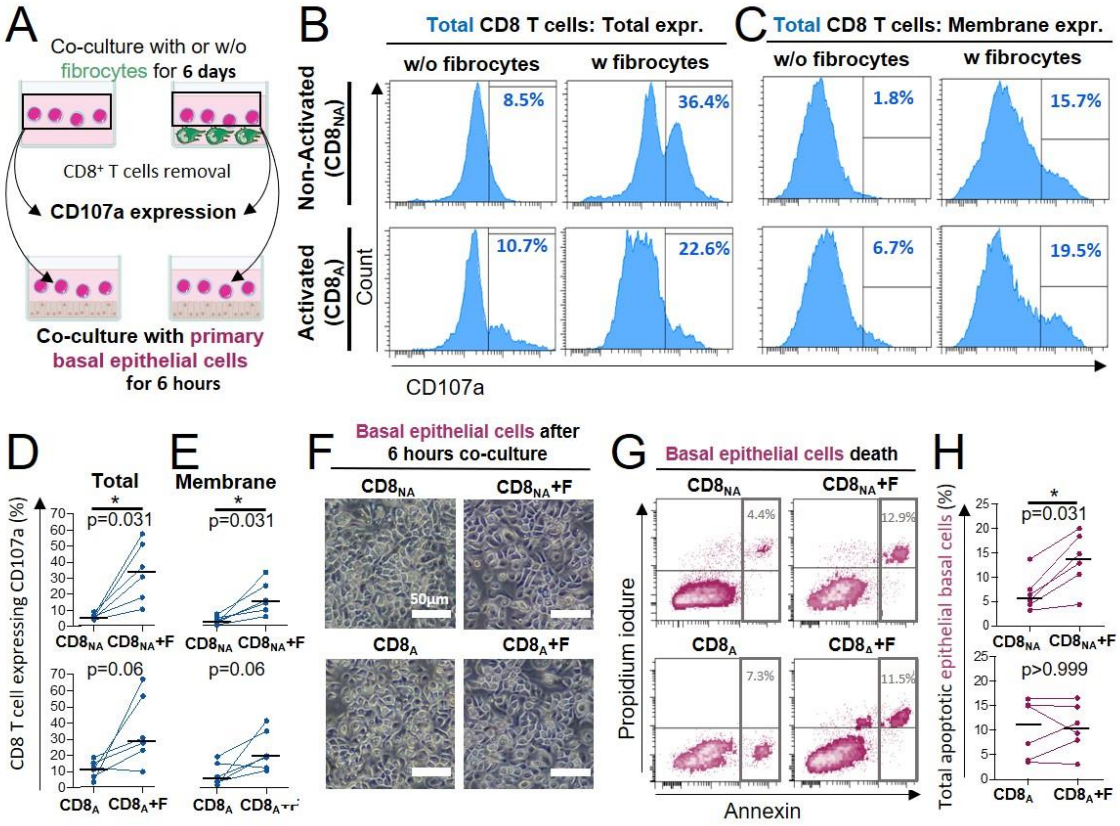

Figure 6. Direct contact between fibrocytes and CD8$^+$ T cells triggers CD8$^+$ T cell cytotoxicity against primary bronchial basal epithelial cells. (**A**) Experiment design: CD8$^+$ T cells have been either non-activated ("CD8$_{NA}$") or activated ("CD8$_A$") before being co-cultured with fibrocytes. 6 days after fibrocytes co-culture, CD8+ T cells were transferred and cultured with primary bronchial basal epithelial cells during 6 hours. (**B**, **C**) Representative gating strategy for identification of CD8 T cells expressing CD107a without (w/o) fibrocytes (left panels) or with (w) fibrocytes (right panels). Histograms represent representative cell count (y-axis) versus CD107a fluorescence (x-axis) for total (**B**) and

extracellular expression (**C**). (**D**, **E**) Comparison of quantifications of $CD8^+$ T cells expressing the CD107a, removed from co-culture without fibrocyte ("CD8") and with fibrocyte ("CD8+F") for total (**D**) and extracellular (**E**) expressions. (**F**) Representative brightfield images of primary basal epithelial cells co-cultured with $CD8^+$ T cells for 6 hours, following their previous co-culture without (CD8) or with fibrocytes (CD8+F) for 6 days. (**G**) Representative gating strategy for identification of apoptotic primary bronchial epithelial basal cells exposed to $CD8^+$ T cells which were previously co-cultured without (CD8, left panel) or with fibrocytes (CD8+F, right panel). Dot plots represents representative Propidium iodure fluorescence (y-axis) versus Annexin fluorescence (x-axis). (**H**) Comparison of quantifications of apoptotic primary bronchial epithelial basal cells exposed to CD8 T cells which were previously co-cultured without (CD8) or with fibrocytes (CD8+F). (**D**, **E**, **H**) Medians are represented as horizontal lines. * $P < 0.05$, Wilcoxon matched paired tests.

Direct contact with CD8+ T cells triggers fibrocyte engagement towards immunologic signaling.

To analyze the effect of the interaction on the fibrocyte, we performed proteomic analyses on fibrocytes, alone or in co-culture during 6 days with $CD8^+$ T cells either non-activated or activated (Figure 7A). Of the top ten pathways that were most significantly activated in co-cultured vs mono-cultured fibrocytes, largest upregulated genes were those of the dendritic cell maturation box, the multiple sclerosis signaling pathway, the neuroinflammation signaling pathway and the macrophage classical signaling pathway, irrespective of the activation state of $CD8^+$ T cells (Figure 7B). The changes were globally identical in the two conditions of $CD8^+$ T cell activation, with some upregulation more pronounced in the activated condition. They were mostly driven by up-regulation of a core set of Major Histocompatibility Complex class I (HLA-B, C, F) and II (HLA-DMB, DPA1, DPB1, DRA, DRB1, DRB3) molecules, co-simulatory and adhesion molecules (CD40, CD86 and CD54). Another notable proteomic signature was that of increased expression of IFN signaling-mediators IKBE and STAT1, and the IFN-responsive genes GBP2, GBP4 and RNF213. We also observed a strong downregulation of CD14, suggesting fibrocyte differentiation, and an upregulation of the matrix metalloproteinase-9 (MMP9) in the non-activated condition only. these changes suggest that the interaction between $CD8^+$ T cells

and fibrocytes promotes the development of fibrocyte immune properties, which could subsequently impact the activation of $CD4^+$ T cells activation.

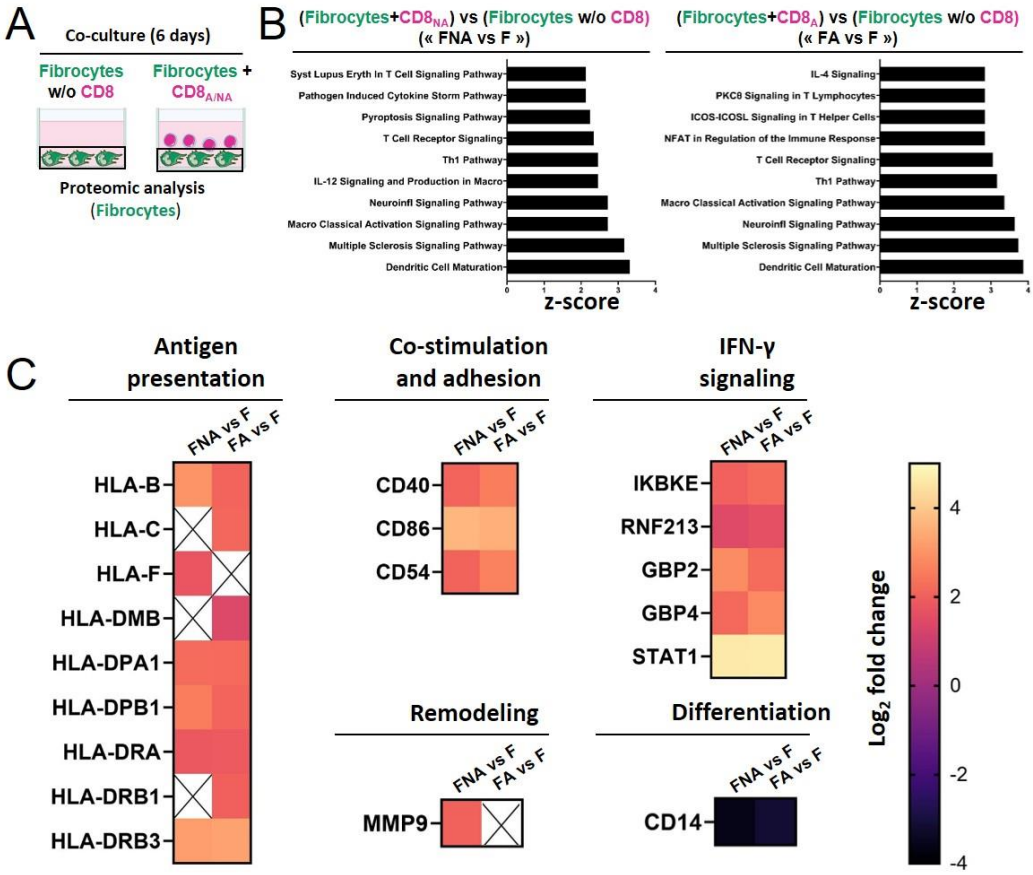

Figure 7. Direct contact between fibrocytes and $CD8^+$ T cells favors the acquisition of fibrocyte immune properties. (**A**) Experiment design: fibrocytes have been either cultured alone, or with $CD8^+$ T cells that have been previously non-activated ("$CD8_{NA}$") or activated ("$CD8_A$"). After 6 days of (co)-culture, fibrocyte proteins have been extracted for proteomic analyses. (**B**) Top 10 Canonical Ingenuity Pathways significantly altered in fibrocytes co-cultured with non-activated CD8+ T cells or activated CD8+ T cells *vs* fibrocytes cultured alone ("FNA *vs* F", left graph, "FA *vs* F", right graph, respectively, n=4 for each condition), ranked by Z-score, obtained by Gene Set Enrichment Analysis. (C) Heatmaps of significantly differentially regulated proteins in FNA *vs* F and FA *vs* F, including proteins related to antigen presentation, co-stimulation and adhesion, remodeling, IFN-γ signaling and differentiation. The color scale indicates the $\log_2$ fold changes of abundance for each protein.

Stochastic mathematical model taking into account intercellular interactions describes the evolution over time of cell populations in control and COPD bronchi

All the above mentioned results led us to hypothesize that fibrocyte infiltration into the lung, differential migration of fibrocytes towards $CD8^+$ T cells and subsequent $CD8^+$ T cell proliferation, could result in a distinct spatial cellular repartition observed in tissues obtained from patients with COPD, compared to control tissues. To investigate this hypothesis, which could not be experimentally tested, we developed an agent-based (cellular automata) model with local and random cellular interactions. We considered the lamina propria (*i.e.*, the peribronchial zone), located between the bronchial epithelium and the smooth muscle layer, which contains fibrocytes and $CD8^+$ T cells. In line with the present analysis, the computational domain (*i.e.*, the lamina propria), corresponds to a zone of 179 000 μm^2. Fibrocytes and $CD8^+$ T cell are considered as individual objects that can move, divide, die and infiltrate the lamina propria at the stable state and during exacerbation. Their individual behaviors and interactions are supposed to be stochastic and the value of the probabilities has been established from literature (Afroj et al., 2021; Bivas-Benita et al., 2013; Dupin et al., 2016, 2019; Ely et al., 2006; Freeman et al., 2007; Gribben et al., 1995; Hurst et al., 2010; Ling et al., 2019; McMaster et al., 2015; Mrass et al., 2017; Saetta et al., 1999; Scheipers & Reiser, 1998; Schmidt et al., 2003; Schyns et al., 2019; Siena et al., 2011; Takamura et al., 2016; Zenke et al., 2020) and the present *in vitro* data, as summarized in the method section and in Tables S9 and S10, and exhaustively described in the supplementary text and (Dupin, Eyraud, et al., 2023). Initial cell densities were scaled with respect to reference values, corresponding to the mean densities measured in non-smoking subjects. Simulations started with these initial densities and ended 20 years later, to reflect the average time between the beginning of cigarette smoke exposure and COPD onset (Løkke et al., 2006).

All the biological processes are governed by probabilities (Figure 8A). $CD8^+$ T cells, but not fibrocytes, are able to proliferate, based on our own unpublished observations and other

studies (Ling et al., 2019; Schmidt et al., 2003). The presence of fibrocytes in the local neighbourhood of a $CD8^+$ T cell can trigger $CD8^+$ T cell division with an increased probability, based on the present *in vitro* experiments showing that the contact between those two cell types greatly enhanced $CD8^+$ T cell proliferation. When a $CD8^+$ T cell has many other T cells in its neighbourhood, it can die with an increased probability, in agreement with (Zenke et al., 2020) and our *in vitro* results. Fibrocytes and $CD8^+$ T cells movements depend on the local neighbourhood of cells, reflecting their relative chemo-attractive properties. We then simulated the evolution over 20 years, with two sets of parameters, respectively for the control and COPD cases and the second for the COPD case (see supplementary text).

We first tested the results of simulations against our experimental data from patients' tissues. First, we compared cell densities, experimentally measured in tissue samples, with theoretical predictions at the final state. Snapshots of the peribronchial area at the end of the simulations show that the densities of cells as well as their relative distribution were different between healthy and COPD situations (Figure 8B). From the simulations (n=160 in each condition), we found a median of 754 $CD8^+$ T cells/mm^2 (95% CI, 748 to 763) and 106 fibrocytes/mm^2 (95% CI, 101 to 108) in the control situation, and 1187 $CD8^+$ T cells/mm^2 (95% CI, 1169 to 1195) and 212 fibrocytes/mm^2 (95% CI, 206 to 216) in the COPD situation. These values are in very good agreement with our experimental findings, and the simulations were also able to reproduce the statistical increase of cell densities in COPD situation compared to that of controls (Figure 8C). Next, we tested if our theory accounted for the experimental relative distribution of $CD8^+$ T cells and fibrocytes. The densities of $CD8^+$ T cells in interaction with fibrocytes (Figure 8D), the mean minimal distances between fibrocytes and $CD8^+$ cells (Figure 8E), the distribution of mean minimal distances (Figure S13) and the mean number of mixed cell clusters (Figure 8F) were in good

agreement with tissular analyses and mimicked the variations observed between control subjects and patients with COPD. The densities of mixed cell clusters predicted by simulations (control simulations: median = 17 clusters/mm^2 (95% CI, 18 to 21), COPD simulations: median = 45 clusters/mm^2 (95% CI, 46 to 51), P<0.001) agreed perfectly with experimental measurements (Figure 8G) and were therefore chosen as a readout of intercellular interactions in the following analyses. If purely random, the density of mixed clusters was expected to be 28 clusters/µm^2 (95% CI, 25 to 29) and 73 clusters/µm^2 (95% CI, 70 to 74) in control and COPD situations, respectively (Figure S14). These random densities as well as the others parameters quantifying the relative distribution of cells were statistically different from the distributions obtained in both simulations and *in situ* analyses (Figure S14). We conclude that the relative organization of CD8$^+$ T cells and fibrocytes in control and COPD bronchi did not result from a pure stochastic mechanism but implicates chemotaxis processes.

One of the strengths of the model is to allow the monitoring of the temporal evolution of the different cellular processes and the numerical detection of a change of regime (Figure 8H-I). CD8$^+$ T cells infiltration remained identical in control and COPD situation. Fibrocyte-induced T cell proliferation, that represents the minor part of the total proliferation in control situation, quickly increased in COPD situation over time to reach a plateau after approximately 4 years. As the basal proliferation of CD8$^+$ T cells remained similar in healthy and diseased situations, the resulting total proliferation in CD8$^+$ T cells over time was higher in the COPD situation compared to the control one. COPD dynamics also affected CD8$^+$ T cell death, with a concomitant increase of T cell-induced death. In total, the net balance between gain and loss of CD8$^+$ T cells was around zero for control dynamics and strictly positive for COPD dynamics, explaining the increased CD8$^+$ T cell density in COPD simulations. Fibrocytes infiltration remained very similar in control and

COPD dynamics (Figure 8I). Fibrocytes death was initially lower in COPD simulations before increasing and reaching a stationary state after approximately 7 years, resulting in a net expansion of fibrocytes population in COPD bronchi after 20 years. Moreover, the simulations allowed us to monitor the interactions between fibrocytes and $CD8^+$ T cells. The density of mixed cell clusters gradually increased in the first years of the COPD simulation before reaching a stationary state after approximately 6 years (Figure 8J, Movies S2 to S5). Altogether, the theory of the influence of local interactions tested by our agent-based (cellular automata) model correctly accounts for the shift of absolute and relative distribution of $CD8^+$ T cells and fibrocytes in peribronchial areas from control subjects to patients with COPD.

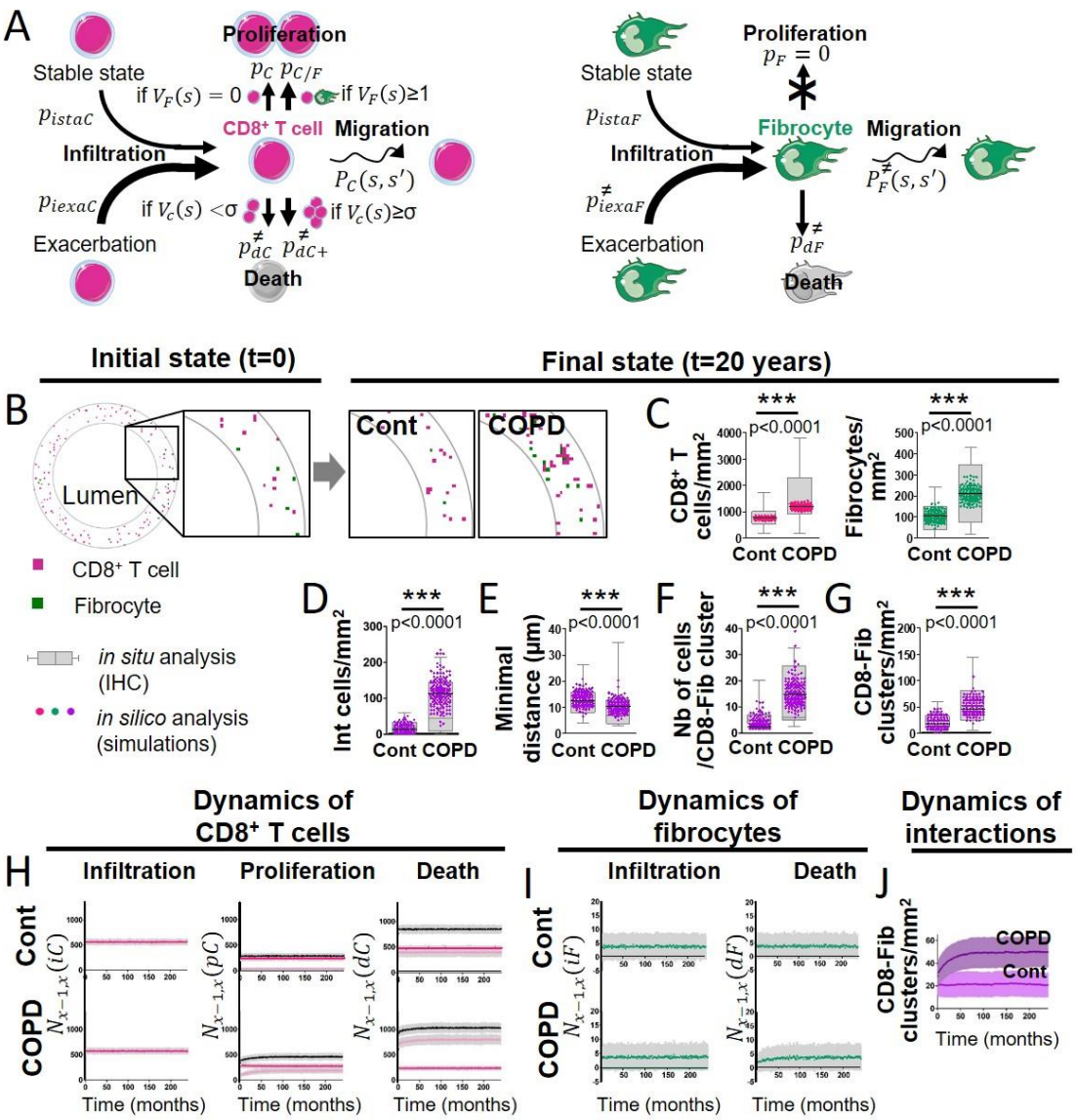

Figure 8. A probabilistic cellular automata type model captures the features of the normal and pathological patterns of cell organisation observed in the tissues. (A) Schematic representation of the probabilities associated with CD8$^+$ T cells (left panel) and fibrocytes (right panel). For each CD8$^+$ T cell, we define a "basal" probability p_{dC} of dying, an increased probability p_{dC+} of dying when the CD8$^+$ T cell has many other CD8$^+$ T cells in its neighborhood, a "basal" probability p_C of dividing, an increased probability $p_{C/F}$ of dividing when the CD8$^+$ T cell has fibrocytes in its neighborhood, a probability $P_C\,(s,s')$ of moving from a site s to a neighboring site s', a probability p_{istaF} to be infiltrated at the stable state and a probability p_{iexaC} to be infiltrated during exacerbation. For each fibrocyte, we define a probability p_{dF} of dying, a probability p_F of dividing, a probability $P_F\,(s,s')$ of moving from a site s to a neighboring site s', a probability p_{istaF} to be infiltrated at the stable state and a probability p_{iexaF} to be infiltrated during exacerbation. The ≠ symbol indicates parameters whose numerical value differs from control to COPD situation. **(B)** Selected representative pictures for initial state and final states after 20 years of control and COPD dynamics. Images surrounded by black squares: higher magnifications of peribronchial area. CD8$^+$ T cells and fibrocytes are represented respectively by pink and green squares. **(C)** CD8$^+$ T cells (left) and fibrocyte (right) densities. **(D)** Interacting cells densities of

interacting cells. (**E**) Mean minimal distances between fibrocyte and CD8$^+$ T cells. (**F**) CD8$^+$ T cells-fibrocytes-containing clusters ("CD8-Fib clusters") densities. (**G**) mean number of cells by CD8-Fib clusters. (**C-G**), n=160 simulations for each situation. The medians are represented as horizontal lines. The equivalent measurements measured on patient's tissues are represented by gray boxes (25th to the 75th percentile) and whiskers (min to max). ***: P<0.001. unpaired t-tests or Mann-Whitney tests. (**H**, **I**) Mean kinetics of the populations of CD8$^+$ T cells and fibrocytes in control and COPD situation *in silico*. Standard deviations are indicated in gray, n=160 simulations. Left panels: $N_{x-1,x}(iC)$ and $N_{x-1,x}(iF)$ are the number of CD8$^+$ T cells (resp. fibrocytes) that have infiltrated the peribronchial area for the month x, relatively to the surface of interest. For fibrocytes, the infiltration at the stable state and during exacerbation are indicated respectively in green and light green. For control situation, there is no infiltration by exacerbation. Midde panels: $N_{x-1,x}(pC)$ is the number of CD8$^+$ T cells that have proliferated for the month x, relatively to the surface of interest. Basal duplication, fibrocyte-induced duplication and total duplication are indicated respectively in pink, light pink and black. Right panels: $N_{x-1,x}(dC)$ and $N_{x-1,x}(dF)$ are the number of CD8$^+$ T cells (resp. fibrocytes) that have died for the month x, relatively to the surface of interest. For CD8$^+$ T cells, basal death, T cell-induced death and total death are indicated respectively in pink, light pink and black. (**J**) Graphs showing the variations of the mean densities of CD8-Fib clusters over time in control (light purple) and COPD situation (dark purple).

Simulations help to predict the outcomes of therapeutic strategies

We performed additional simulations to investigate the outcomes of possible therapeutic interventions. First, we applied a COPD dynamics during 20 years, to generate the COPD states, that provide the basis for treatment implementation. Then, we applied a COPD dynamics during 7 years, that mimics the placebo condition (Figure 9A), that we compared to a control dynamics ("Total inhibition"), that mimics an ideal treatment able to restore all cellular processes. As expected the populations of fibrocytes and CD8$^+$ T cells, as well as the density of mixed clusters, decreased. These numbers reached levels similar of healthy subjects after approximately 2.5 years, and this time point can therefore be considered as the steady state (Figure 9B-E). Monitoring of the different processes revealed that these effects were mainly due to a reduction in fibrocyte-induced CD8$^+$ T duplication, and a transient or more prolonged increase in basal fibrocyte and CD8$^+$ T death (Figure 9C-D). Then, three possible realistic treatments were considered (Figure 9A). We tested the effect of directly inhibiting the interaction between fibrocytes and CD8$^+$ T cells by blocking CD54.

This was implemented in the model by altering the increased probability of a $CD8^+$ T cell to divide when a fibrocyte is in its neighbourhood, as shown by the co-culture results (Figure 4). We also chose to reflect the effect of a dual CXCR1/2 inhibition by setting the displacement function of fibrocyte similar to that of control dynamics, in agreement with the *in vitro* experiments (Figure 2E). Blocking CD54 only slightly reduced the density of $CD8^+$ T cells compared to the placebo condition, and had no effect on fibrocyte and mixed cluster densities (Figure 9B). CXCR1/2 inhibition was a little bit more potent on the reduction of $CD8^+$ T cells than CD54 inhibition, and it also significantly decreased the density of mixed clusters (Figure 9B). As expected, this occurred through a reduction of fibrocyte-induced duplication, which was affected more strongly by CXCR1/2 blockage than by CD54 blockage (Figure 9C-E). Combining both therapies (CD54 and CXCR1/2 inhibition) did not strongly major the effects (Figure 9B-E). In all the conditions tested, the size of the fibrocyte population remained unchanged, suggesting that other processes such as fibrocyte death or infiltration should be targeted to expect broader effects.

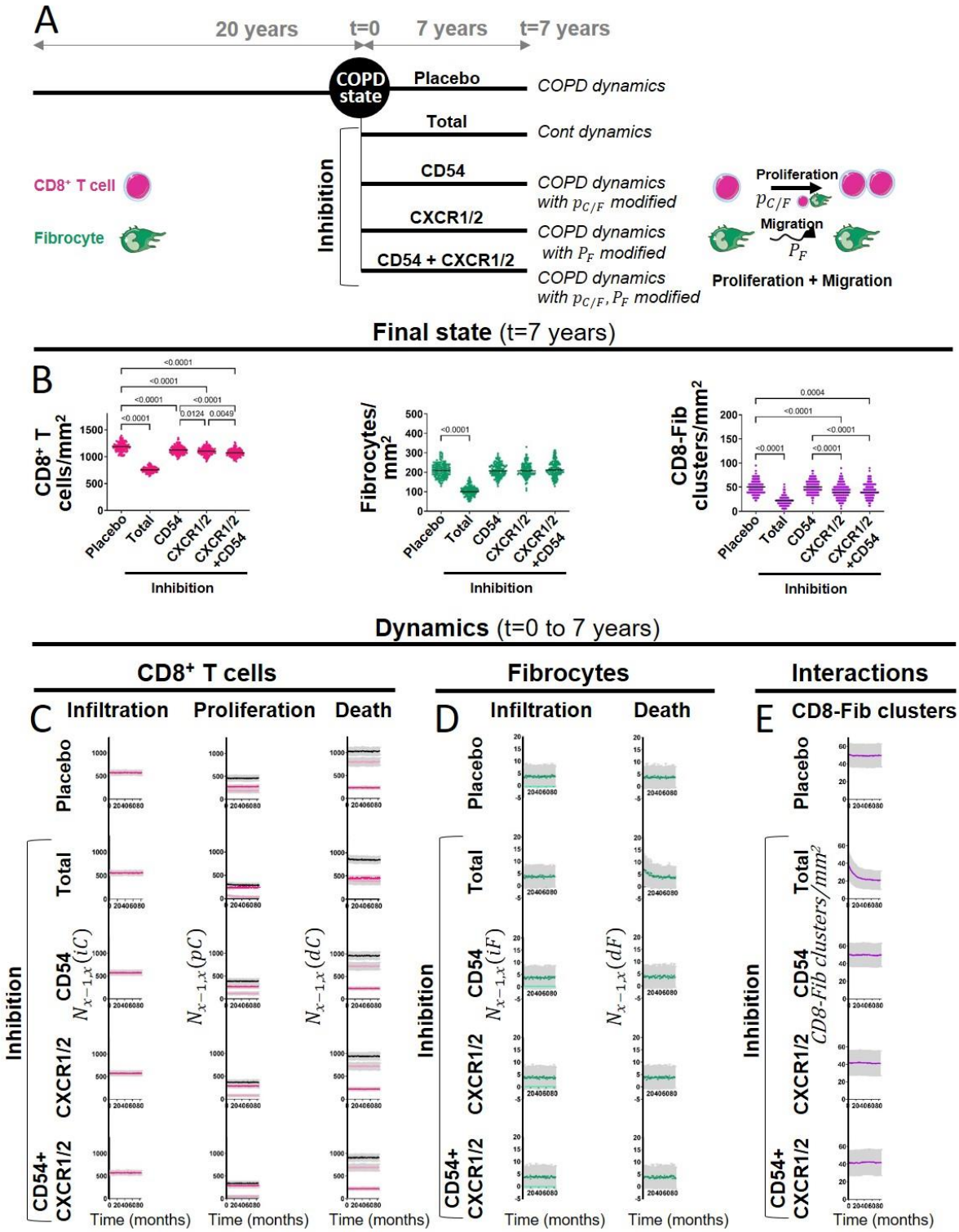

Figure 9. The outcomes of therapeutic interventions are be predicted by simulations. (**A**) Schematic representation of the design used to test therapeutic strategies. COPD states were first generated by applying COPD dynamics during 20 years (n=144 simulations). Then, different dynamics were applied during 7 years: a COPD dynamics (corresponding to the placebo condition), a control dynamics (corresponding to an ideal treatment able to restore all cellular processes, "Total inhibition"), and modified COPD dynamics (corresponding to CD54, CXCR1/2 and dual inhibitions with alterations of the probability

$p_{C/F}$ of dividing when the CD8$^+$ T cell has fibrocytes in its neighbourhood, the probability P_F for a fibrocyte to move, and both, respectively). (**B**) CD8$^+$ T cells (left), fibrocyte (middle) and CD8$^+$ T cells-fibrocytes-containing clusters ("CD8-Fib clusters", right) densities at the final state (t=7 years). The medians are represented as horizontal lines. One-way ANOVA with Tukey's post-tests. P-values below 0.05 with Tukey's post-tests are indicated on the graphs, except for the comparisons between the condition "Total inhibition" and the other conditions of inhibition, that are not indicated. (**C-D**) Mean kinetics of the populations of CD8$^+$ T cells and fibrocytes in the different conditions (t=0 to 7 years). Left panels: $N_{x-1,x}(iC)$ and $N_{x-1,x}(iF)$ are the number of CD8$^+$ T cells (resp. fibrocytes) that have infiltrated the peribronchial area for the month x, relatively to the surface of interest. For fibrocytes, the infiltration at the stable state and during exacerbation are indicated respectively in green and light green. For the total inhibition situation, there is no infiltration by exacerbation. Midde panels: $N_{x-1,x}(pC)$ is the number of CD8$^+$ T cells that have proliferated for the month x, relatively to the surface of interest. Basal duplication, fibrocyte-induced duplication and total duplication are indicated respectively in pink, light pink and black. Right panels: $N_{x-1,x}(dC)$ and $N_{x-1,x}(dF)$ are the number of CD8$^+$ T cells (resp. fibrocytes) that have died for the month x, relatively to the surface of interest. For CD8$^+$ T cells, basal death, T cell-induced death and total death are indicated respectively in pink, light pink and black. (**E**) Mean kinetics of the densities of CD8-Fib clusters in the different conditions (t=0 to 7 years). (**C-E**) Standard deviations are indicated in gray, n=144 simulations.

Discussion

The present study aimed at identifying the role and mechanism of fibrocyte-CD8$^+$ T cells cross-talk in COPD. A previous study had pointed out a pivotal role for fibrocyte to activate CD8$^+$ T cells proliferation (Afroj et al., 2021). However, whether and how both cell types could interact in bronchi, as well as their implication in COPD was completely unknown. Quantitative image analysis provided crucial insight into the relative distribution of fibrocytes and CD8$^+$ T cells in distal bronchial specimens from control subjects and COPD patients. In addition to data from previous studies demonstrating that the densities of both fibrocytes (Dupin et al., 2019) and CD8$^+$ T cells (Saetta et al., 1999) are increased within the distal bronchi of COPD patients, we found that fibrocyte and CD8$^+$ T cells are localized in close proximity in peribronchial areas, especially in tissues from patients with COPD. We deciphered the spatiotemporal characteristics of these cell–cell contacts by live imaging in an *in vitro* autologous co-culture assay, and showed that the duration of the contacts was

compatible with activation through the establishment of dynamic synapses. On the one hand, CD8$^+$ T cells induced fibrocyte chemotaxis through CXCL8/CXCR1/2 axis and engagement towards immunologic signaling, and, on the other hand, fibrocytes directly induced CD8$^+$ T cell proliferation, cytokine production and cytotoxic activity against bronchial epithelial cells (Figure 10). The strength of our work relies on the integration of findings from the present *in vitro* experiments and other studies into a comprehensive computational model that provides an accurate prediction of histological *ex vivo* characteristics and the possibility to figure out the *in vivo* effect of drugs. Altogether, our data suggest a pivotal role for fibrocytes to activate CD8$^+$ T cell deleterious functions in the context of COPD.

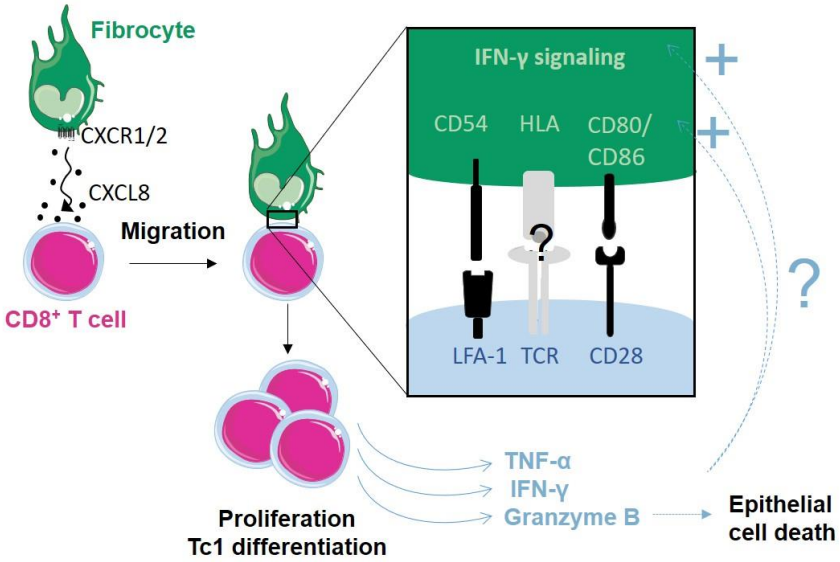

Figure 10. Proposed model of how fibrocytes interact with CD8$^+$ T cells in the context of COPD. Fibrocyte chemotaxis towards CD8$^+$ T cells is mainly due to an increased CXCL8 secretion by CD8$^+$ T cells in COPD lungs, and promotes direct contact between both cell types. This interaction triggers CD8$^+$ T cell proliferation, cytokine production and cytotoxic activity. The interaction and its consequences might be further increased by a reinforcement of IFN-γ signaling and expression of molecules belonging to the immune synpase, from the fibrocyte side.

We analyzed the relationship between these histological parameters and clinical data and found associations between fibrocyte presence, fibrocyte-CD8$^+$ T cell interaction and the alteration of lung function. We have demonstrated using stepwise and multivariate

regressions that the density of interacting cells and the density of mixed cell cluster were the two best correlated parameters with the FEV_1/FVC ratio, supporting a potential role for the interplay between both cell types in COPD. Since regions of microscopic emphysematous destruction of terminal bronchioles have been associated with increased infiltration of $CD8^+$ T cells and immune response activation, such as the up-regulation of IFN-γ signaling (Xu et al., 2021), and that we have evidenced fibrocyte-mediated cytotoxic activity in $CD8^+$ T cells, it is tempting to speculate that fibrocyte-$CD8^+$ T cell interplay could be implicated in early changes leading to tissue remodeling and chronic inflammation in COPD. Of note, the gene signature obtained by tissue microarray associated with this site also indicates the modification of two genes associated with the tissue repair process, FGF10 and TGFB2 (Xu et al., 2021). Considering the possible effect of $CD8^+$ T cells on fibrocyte differentiation, it could be worthwhile to focus on these genes in further studies.

We also addressed the potential mechanisms explaining these increased interactions of $CD8^+$ T cells and fibrocytes in tissues of COPD patients. Chemotaxis could guide $CD8^+$ T cells towards fibrocytes and reciprocally, as it has been proposed for T cells towards dendritic cells (Mackay, 2001; Ngo et al., 1998; von Andrian & Mackay, 2000). Stronger or longer interactions could also explain the differential spatial distribution between healthy and diseased tissues. On the other hand, the contact between both cell types could also occur through a stochastic mechanism, as shown for $CD4^+$ T cells and dendritic cells in lymph nodes, without any implication of chemotactic processes (Miller et al., 2004). Although we cannot totally rule out a role for fibrocyte-$CD8^+$ T cell adhesion to explain the increased interactions, our findings rather suggest a central role for the CXCL8-CXCR1/2 axis in promoting encounters between $CD8^+$ T cells and fibrocytes in COPD patients. Importantly, this is further supported by the results of computational modelization, which only integrates

chemotaxis and not adhesion processes, revealing a final spatial repartition of cells in the COPD situation distinct from a random distribution. Altogether, our data suggest that the likelihood of interactions between fibrocytes and $CD8^+$ T cells could be increased in tissues from patients with COPD through the CXCL8-CXCR1/2 axis thus participating to cluster fibrocytes and $CD8^+$ T cells in diseased tissues. Importantly, dual blockers of CXCR1-CXCR2 have been suggested as therapeutic targets in COPD (Henrot et al., 2019). Although reparixin, a dual blocker of CXCR1-CXCR2, was efficient in our *in vitro* experiments to block the increased chemotaxis of fibrocytes towards secretion of COPD $CD8^+$ T cells, the *in vivo* effect of this therapy predicted using our computational model was moderate, highlighting the importance of this integrated approach.

We show that fibrocytes act as a major promoter on $CD8^+$ T cell proliferation, thus confirming, in an autologous co-culture system, what has been previously found in the context of cancer-related immunity (Afroj et al., 2021). This is consistent with the present *in situ* analyses, showing the presence of clusters containing both cell types in peribronchial area, especially in the tissues from patients with COPD. The mean numbers of cells in those clusters remained relatively low, suggesting that these structures are distinct from inducible bronchus-associated lymphoid tissue (iBALT) (Conlon et al., 2020). Although a previous report has demonstrated that fibrocytes, exposed to viral antigens, could induce proliferation of naïve $CD8^+$ T cells (Balmelli et al., 2005), the pro-proliferative effect exerted by fibrocytes on $CD8^+$ T cells occurred without antigen exposure in our *in vitro* study. This antigen-independent T cell proliferation driven by fibrocytes was also found in the context of sepsis (Nemzek et al., 2013), suggesting that fibrocytes generally impact T cells expansion with a mechanism independent of the traditional antigen-driven clonal proliferation. This is also in agreement with our findings showing that contacts between

CD8$^+$ T cells and fibrocytes were relatively short and dynamic, and that the dynamics of the interaction did not depend on the activation state of CD8$^+$ T cells. The spatiotemporal behavior of CD8$^+$ T cells was consistent with the establishment of dynamic synapse, also called "kinapse" (Dustin, 2008), which are associated with the induction of relatively weak TCR signals (Moreau et al., 2012). We have evidenced the requirement for cellular contacts, implicating the surface receptors CD86 and CD54. The lack of effect of the anti-CD86 and CD54 in pre-activated CD8$^+$ T cells might indicate potential changes of expression of molecules belonging to the immunological synapse upon activation, that could make the lymphocytes more responsive to others signals. The well-known inhaled glucocorticoids (*i.e.*, budesonide and fluticasone propionate) also failed to significantly inhibit fibrocyte-induced CD8$^+$ T cell proliferation. This is consistent with their lack of activity in lymphocytes obtained from patients with COPD (Kaur et al., 2012). In contrast, we propose that targeting the interaction between structural and immune cells and/or its consequences should reveal robust candidates for future pharmacotherapeutic strategies to treat COPD. Of note, the stimulatory activity of CD8$^+$ T cells by fibrocytes was also found to be enhanced by the blockade of the PD-1/PD-L1 pathway in a previous study (Afroj et al., 2021). As this latter property of fibrocytes may be beneficial in tumor microenvironment (Henrot et al., 2021), especially when cancer patients were treated with anti–PD-1/PD-L1 antibody, it might be rather detrimental in COPD patients, by promoting tissue damages and chronic immune inflammation.

Fibrocytes skewed CD8$^+$ T-cell populations towards both CD8^{high} and CD8^{low} phenotypes in a cell–cell contact independent manner. It has been described that, following contact between an antigen presenting cell and a lymphocyte, asymmetric division can occur generating a memory cell, weakly expressing CD8, and an effector cell strongly expressing

CD8 (Backer et al., 2018; J. T. Chang et al., 2007). The asymmetry is reduced but still present even without specific recognition of foreign antigen by T cells (J. T. Chang et al., 2007). It is tempting to speculate that the induced proliferation we observed in our experiments generates, via asymmetric division, unequal CD8 inheritance in daughter cells. The low level of cytokine expression in $CD8^{low}$ cells is compatible with an exhausted phenotype, while $CD8^{high}$ cells express higher levels of cytokines, a profile consistent with an effector commitment. Although the presence of the $CD8^{high}$ and $CD8^{low}$ subsets remain to be evidenced in the tissues, we suspect that the relative expansion of the $CD8^{high}$ and $CD8^{low}$ subset triggered by fibrocytes could have functional implications. Reiterative rounds of $CD8^{+}$ T cells division induced by frequent interactions with fibrocytes might induce defective immune response by exhausted $CD8^{low}$ T cells (Grundy et al., 2013; McKendry et al., 2016), and tissue destruction by cytotoxic $CD8^{high}$ cells (Chrysofakis et al., 2004; Maeno et al., 2007).

In COPD, outside of exacerbations, factors triggering pro-inflammatory cytokines production are still elusive. Here, we demonstrate that fibrocytes exert a strong effect through soluble factors and direct cellular contacts with $CD8^{+}$ T cells, inducing a massive upregulation of TNF-α, IFN-γ and granzyme B production, all implicated in COPD pathophysiology (Barnes, 2016). Greater production of TNF-α, IFN-γ and granzyme B by $CD8^{+}$ T cells triggered by the interaction with fibrocytes is consistent with previous studies showing enhanced production of Tc1 cytokines and cytotoxic molecules by $CD8^{+}$ T cells purified from patients with COPD (Freeman et al., 2010; Hodge et al., 2007; Lethbridge et al., 2010), suggesting that local interactions with cells such as fibrocytes may play a pivotal role in CD8 polarization in COPD. In particular, TNF-α has proinflammatory and prooxidative actions (Mukhopadhyay et al., 2006), and its overexpression has been

associated with emphysema (Lundblad et al., 2005). TNF-α can directly contribute to cytolysis, together with the cytotoxic granzyme B (Velotti et al., 2020) and in synergy with IFN-γ (Williamson et al., 1983). TNF-α can also indirectly participate to extracellular matrix degradation through the induction of matrix metalloproteinases (Wright et al., 2007). Simultaneously, the production of the pro-fibrotic IL-17 was also induced upon co-culture with fibrocytes, raising the possibility that the interaction between $CD8^+$ T cells and fibrocyte participates to the generation of IL-17-secreting $CD8^+$ T cells in airways of patients with COPD (Y. Chang et al., 2011). Interestingly, IL-17 is able to simulate matrix components synthesis in other cell types, including fibrocytes, and promotes CD40-mediated IL-6 production by fibrocytes (Hayashi et al., 2013). Up-regulated pathways identified in proteomic profile of fibrocytes co-cultured with $CD8^+$ T cells are very consistent with a shift towards a proinflammatory phenotype rather than towards a reparative role. The activation of IFN-γ signaling could be triggered by $CD8^+$ T cell secretion of IFN upon fibrocyte interaction, suggesting the existence of a positive feedback loop (Figure 10). Additionally, the priming of fibrocytes by $CD8^+$ T cells could also induce $CD4^+$ T cell activation. Cooperative interactions between fibrocytes and $CD8^+$ T cells, through tissue destruction and abnormal inflammation, may thus directly contribute to the loss of normal lung function. On the other hand, $CD8^+$ T cell production of anti-inflammatory cytokines such as IL-10, was also stimulated upon co-culture with fibrocytes. In total, rather than the net production of each cytokine, it is probably the balance or imbalance between pro-inflammatory and anti-inflammatory molecules that will dictate the outcome of the inflammatory process.

Whereas the field of respiratory research is rapidly moving towards an exhaustive description of modifications of molecular and cellular components in diseased lungs, the

actual transition between a healthy to a diseased state, although critical, remains very difficult to investigate. We developed here a probabilistic cellular automata type model to explore of dynamic behaviors and interactions between fibrocytes and $CD8^+$ T cells. Previous agent-based computational approaches have been used to describe the switch from normal to allergic response (Pothen et al., 2015) and airway remodeling in asthma (Saunders et al., 2019), but, to our knowledge, this type of modeling was never applied to COPD. Qualitative estimates of probabilities that govern cell death, proliferation, infiltration and displacement are derived from experimental data from our study and others. We could simulate spatiotemporal behaviors of cells in the lamina propria over long period of time (*i.e.*, 20 years) and we showed that this model can accurately reproduce the absolute and relative repartition of fibrocytes and $CD8^+$ T cells in both control and COPD situations.

Although simulated and *in situ* data were close, the variances of *in silico* data were smaller than the *in situ* measurements, which can be probably explained by the fact that cell diversity and interactions are far more complex that those considered in this model. Nevertheless, it appears that (i) our model captures important aspect of reality, and (ii) modifications of specific cellular processes and local interactions, *i.e.* fibrocyte-induced $CD8^+$ T cell proliferation and fibrocyte attraction towards $CD8^+$ T cells, are sufficient to reproduce the shift of histological composition between the control and COPD situations. This theoretical approach and associated simulations allowed us to validate the key hypothesis of modification of local interactions, and to show that that the specific values of the COPD parameters led to an increased cell density and the spatial patterns observed in patients with COPD. The simulations made it possible to follow over time various quantities of interest and to empirically determine the time when the stationary state is achieved, that would be difficult to reveal in any other way. Given the consistency of our results with those from the literature, our model provides a unique opportunity to decipher the dynamics of increased

interactions between the two cell types as well as the infinite possibility to investigate therapeutic strategies. Using the simulations, we were indeed able to estimate the characteristic time to reach a stationary state reminiscent of a resolution of the COPD condition. This time of approximately 2.5 years was totally unpredictable by *in vitro* experiments, and indicates that a treatment aiming at restoring these cellular processes should be continued during several years to obtain significant changes.

Regarding potential therapeutic strategies, chemokine-receptor based therapies could be used to inhibit fibrocyte recruitment into the lungs, such as CXCR4 blockade. We have very recently shown that using the CXCR4 antagonist, plerixafor, alleviates bronchial obstruction and reduces peri-bronchial fibrocytes density (Dupin, Henrot, et al., 2023). Because CXCR4 expression in human fibrocytes is dependent on mTOR signaling and is inhibited by rapamycin *in vitro* (Mehrad et al., 2009), alternative strategies consisting of targeting fibrocytes via mTOR have been proposed. This target has proven effective in bronchiolitis obliterans, idiopathic pulmonary fibrosis, and thyroid-associated ophthalmopathy, using rapamycin (Gillen et al., 2013; Mehrad et al., 2009), sirolimus (Manjarres et al., 2023) or an insulin-like growth factor-1 (IGF-I) receptor blocking antibody (Douglas et al., 2020; Smith et al., 2017). Inhibiting mTOR is also expected to have effects on $CD8^+$ T cells, ranging from an immunostimulatory effect by activation of memory $CD8^+$ T-cell formation, to an immunosuppressive effect by inhibition of T cell proliferation (Araki et al., 2010). Last, chemokine-receptor base therapies could also include strategies to inhibit the $CD8^+$-induced fibrocyte chemotaxis, such as dual CXCR1-CXCR2 blockade, which we were able to test in our mathematical model. Immunotherapies directly targeting the interaction between fibrocytes and $CD8^+$ T cells could also be considered, such as CD86 or CD54 blockade. The use of abatacept and

belatacept, that interfere with T cell co-stimulation, is effective in patients with rheumatoid arthritis (Pombo-Suarez & Gomez-Reino, 2019) and in kidney-transplant recipients (Vincenti et al., 2016), respectively. Targeting the IGF-I receptor by teprotumumab in the context of thyroid-associated ophthalmopathy also improved disease outcomes, possibly by altering fibrocyte-T cell interactions (R. J. Bucala, 2022; Fernando et al., 2021). Of note, the outcomes of CXCR1/2 and CD54 blocking strategy for COPD treatment were tested by our simulations, with limited beneficial effects. It suggests that such treatments may be more effective when used in combination with other drugs *e.g.* those affecting fibrocyte infiltration and/or death. Such therapies should be used with caution as they may favour adverse events such as infections, particularly in the COPD population (Rozelle & Genovese, 2007). Additionally, the fibrocytes-lymphocytes interaction has recently been shown to promote anti-tumoral immunity via the PD1-PDL1 immunological synapse (Afroj et al., 2021; Mitsuhashi et al., 2023). Therefore, care should be taken in the selection of patients to be treated and/or timing of treatment administration with regards to the increased risk of lung cancer in COPD patients.

The present *in vitro* model has limitations, including the use of circulating cells for some *in vitro* experiments, that were obtained exclusively from patients with COPD. In particular, it was not possible to test the hypothesis of a different baseline activation state in the blood of patients with COPD in comparison with healthy subjects, that could participate to initiate or maintain the vicious cycle of inflammation. One should also mention the difficulty in extrapolating results obtained from these *in vitro* assays to *in vivo* processes. However, we took this limit into account in our modelization approach, by using a combination of our experiments and measurements obtained in tissues, to accurately determine the dedicated parameters (Dupin, Eyraud, et al., 2023). Even if computational modelization was done in 2D, whereas the bronchi are 3D structures, we believe that our model is representative as it

mimics the cellular distribution of normal and pathological airways, that was also quantified in 2D lung sections. Besides this, some quantitative features of our approach are still valid in 3D, such as the probabilities that govern cell death, proliferation and infiltration, whereas others are expected to change with dimensionality, such as displacement rules.

From our study and others (Hufford et al., 2011; Takamura et al., 2019), it is now clear that the fate of $CD8^+$ T cells in distal airways may depend on multiple successive interactions with different cell types, including fibrocytes. We believe that targeting interaction between structural and immune cells should be considered in future drug discovery programs and that computational modelization should help to refine drug priority.

Materials and Methods

Study Populations

Lung tissues for the *in situ* study were obtained from a previously described cohort (Dupin et al., 2019). The study was registered at ClinicalTrials.gov with identifier NCT01692444 ("Fibrochir" study). The study protocol was approved by the research ethics committee ("CPP") and the French National Agency for Medicines and Health Products Safety ("ANSM"). Briefly, subjects more than 40 years of age were eligible for enrolment if they required thoracic lobectomy surgery for cancer (pN0), lung transplantation or lung volume reduction. A total of 17 COPD patients with a clinical diagnosis of COPD according to the GOLD guidelines (*Global Initiative for Chronic Obstructive Lung Disease*, s. d.) and 25 non-COPD subjects ("control subjects") with normal lung function testing (*i.e.*, $FEV_1/FVC > 0.70$) and no chronic symptoms (cough or expectoration) were recruited from the University Hospital of Bordeaux. Due to low quality of some tissue sections, distal bronchial identification or fibrocyte and CD8+ T cell quantification was impossible in 5 control specimens and 5 COPD specimens, which were excluded from the *in situ* analysis. Lung tissues for the purification of tissular $CD8^+$ T cells and basal bronchial epithelial cells were obtained from a separate cohort of patients requiring thoracic lobectomy surgery for nodule or cancer (pN0) (*i.e.*, TUBE, sponsored by the University hospital of Bordeaux, which includes its own local ethic committee (CHUBX 2020/54)). According to the French law and the MR004 regulation, patients received an information form, allowing them to refuse the use of their surgical samples for research. For the purification of tissular $CD8^+$ T cells, a total of 20 patients with COPD and 26 nonsmokers were prospectively recruited from the University Hospital of Bordeaux, according to the GOLD guidelines (*Global Initiative for Chronic Obstructive Lung Disease*, s. d.) (Table S7). For the purification of

basal bronchial epithelial cells, a total of 2 patients were prospectively recruited from the University Hospital of Bordeaux (Table S9).

To study fibrocyte- $CD8^+$ T cells interplay *in vitro*, blood samples were obtained from a separate cohort of COPD patients, (*i.e.*, COBRA (Bronchial Obstruction and Asthma Cohort; sponsored by the French National Institute of Health and Medical Research, INSERM, Ethics committee number: 2008-A00294-51/1), as outpatients in the Clinical Investigation Centre of the University Hospital of Bordeaux (Table S8).

All subjects gave their written informed consent to participate to the studies. The studies received approval from the local or national ethics committees.

Identification of bronchial fibrocytes and $CD8^+$ T cells

Fragments of distal parenchyma were obtained from macroscopically normal lung resection or transplantation material. The samples were embedded in paraffin and sections of 2.5 µm thick were cut, as described previously (Dupin et al., 2019). Sections were deparaffinized through three changes of xylene and through graded alcohols to water. Heat induced antigen retrieval was performed using citrate buffer, pH 6 (Fisher Scientific, Illkirch, France) at 96°C in a Pre-Treatment Module (Agilent, Les Ulis, France). Endogenous peroxidases were blocked for 10 min using hydrogen peroxide treatment (Agilent). Nonspecific binding was minimized by incubating the sections with 4% Goat Serum (Agilent) for 30 min, before CD8 staining, and before the double staining for CD45 and FSP1. First, the sections were stained with rabbit anti-CD8 monoclonal antibody (Fisher Scientific) during 45 min, and then incubated with HRP anti-Rabbit (Nichirei Biosciences). Immunoreactivity was detected by using the DAB System (Agilent). Second, the same sections were stained with mouse anti-CD45 monoclonal antibody (BD Biosciences, San Jose, CA) overnight and then with rabbit anti-FSP1 polyclonal antibody (Agilent) during 45 min. They were incubated

with Alexa568–conjugated anti-Mouse and with Alexa488–conjugated anti-Rabbit (Fisher Scientific) antibodies. Immunoreactivity was detected by fluorescence for FSP1 and CD45 staining.

The sections were imaged using a slide scanner Nanozoomer 2.0HT with fluorescence imaging module (Hamamatsu Photonics, Massy, France) using objective UPS APO 20X NA 0.75 combined to an additional lens 1.75X, leading to a final magnification of 35X. Virtual slides were acquired with a TDI-3CCD camera. Fluorescent acquisitions were done with a mercury lamp (LX2000 200W - Hamamatsu Photonics) and the set of filters adapted for DAPI, Alexa 488 and Alexa 568. Bright field and fluorescence images where acquired with the NDP-scan software (Hamamatsu) and processed with ImageJ.

Quantification of $CD8^+$ T cells was performed, as described in Figure S1A, C. A color deconvolution plugin was used on brightfield image to isolate the signal corresponding to DAB staining. A binary threshold was applied to this grayscale image, followed by a watershed transformation to the segmented image to separate potential neighboring cells (Figure S1C). $CD8^+$ T cells were then automatically counted by recording all the positive particles with an area greater than 64 μm^2. This threshold was empirically determined on our images to select positive cells. Quantification of dual positive cells for FSP1 and CD45 was performed, as described in Figure 1B, D. A binary threshold was applied to fluorescence images corresponding to FSP1 and CD45 stainings. These images were combined using the "AND" function of the Fiji "Image Calculator" to select cells dual positive for FSP1 and CD45 double staining (Figure S1D). This was followed by a watershed transformation to separate potential neighboring cells. These $CD45^+$ $FSP1^+$ cells were then automatically counted by recording all the positive particles with an area greater than 64 μm^2.

Quantification of the density of CD8$^+$ T cells, FSP1$^+$ CD45$^+$ cells and CD8$^+$ T cells in interaction with CD45$^+$ FSP1$^+$ cells

This latter segmented image was then used to quantify CD8$^+$ T cells in interaction with CD45$^+$ FSP1$^+$ cells as described in Figure 1E: each CD8 positive particle with an area greater than 64 µm^2 was enlarged using the dilatation function (4, 8, 10 and 15 pixels dilatation: used to count the cells respectively less than 1.8, 3.6, 4.5 and 6.8 µm apart). This modified image was combined with the segmented image for dual CD45 FSP1 positive staining using the "AND" function of the Fiji "Image Calculator" to select CD8$^+$ T cells in interaction with CD45$^+$ FSP1$^+$ cells. These interacting cells were automatically counted by recording all the positive particles. The lamina propria contour was manually determined on bright field image and the area was calculated. For distal bronchi, the lumen area was also determined and only bronchi less than 2 mm in diameter were analyzed as described previously (Hogg et al., 2004). The densities of CD8$^+$ T cells, FSP1$^+$ CD45$^+$ cells and interacting cells were defined by the ratio between the number of positive cells in the lamina propria divided by lamina propria area. Tissue area and cell measurements were all performed in a blinded fashion for patients' characteristics.

Quantification of the minimal distances between CD45$^+$ FSP1$^+$ cells and CD8$^+$ T cells

The segmented image produced from the DAB staining image was inverted, and a CD8 distance map was built form the latter image (Figure S1F). As a result, the brighter the pixel, the closer the distance from a CD8$^+$ T cell. Conversely, the darker the pixel, the farther away the distance from a CD8$^+$ T cell. On the binary image produced from FSP1 and CD45 staining images, dual positive cells for FSP1 and CD45 were selected in the lamina propria. Each area corresponding to a FSP1$^+$ CD45$^+$ cell was reported on the CD8 distance map, and the minimal gray value in each area was measured and converted to a distance, allowing to

measure the minimal distance between the $CD45^+$ $FSP1^+$ cell and neighboring $CD8^+$ T cells. For each patient, a frequency distribution of all minimal distances (with 7 µm binning) and the mean minimal distance were calculated.

Quantification of cell clusters

On the segmented image with dual CD45 FSP1 positive staining combined with CD8 positive staining, centroids from positive particles located in the lamina propria were connected by a Delaunay triangulation, using a custom freely available ImageJ plugin (Schneider et al., 2012) (Figure S3A-C, https://github.com/flevet/Delaunay_clustering_ImageJ). All triangles sharing one edge with the ROI defining the lamina propria were removed (Figure S3C, left panel). On the remaining triangulation a distance threshold, corresponding to the minimal mean distance between fibrocytes and $CD8^+$ T cells (40 µm) was applied, allowing to select the connections with a distance lower than the threshold distance (Figure S3C, right panel). The number of clusters and their composition were then automatically recorded.

Dataset transcriptomic analysis

The microarray data of tissular $CD8^+$ T cells was downloaded from the Gene Expression Omnibus (http://www.ncbi.nlm.nih.gov/geo/) using a dataset under the accession code GSE61397. Differential expression analysis between patients with COPD and control subjects was performed using the GEO2R interactive web tool. Heatmaps of the expression profiles for genes related to cell adhesion and chemotaxis were visualized with Graphpad Prism 6 software.

Tissular $CD8^+$ T cell purification, culture and secretion profile analyses

After lung parenchyma resection from control or COPD patients (Table S7), samples were finely chopped at room temperature using scissors and then enzymatically dissociated with 40 IU/mL of collagenase (ThermoFisher) in DMEM medium for 45 min at 37°C. The enzymatic reaction was stopped by adding HBSS medium (Hank's Balanced Salt Solution) without calcium and supplemented with 2mM EDTA (Invitrogen, Cergy Pontoise, France). The cell suspension was filtered twice using 100 µm gauze and 70 µm cell strainer (Fisher Scientific). Tissular $CD8^+$ T cells were purified by positive selecting using CD8 microbeads (Miltenyi Biotech, Paris, France). Then, tissular $CD8^+$ T cells were resuspended in DMEM supplemented with 8% fetal calf serum, soluble anti-CD3 and anti-CD28 antibodies (respectively 1µg and 3µg for 10^6 cells) for a final concentration of 0.5 x 10^6 cells/mL. After 36h, supernatants from tissular $CD8^+$ T cells were collected and frozen, for migration experiments or for further analyses. Supernatants from different samples obtained either from non-smoking subjects or patients from COPD were pooled for migration experiments. Supernatant concentrations of CXCL1, CXCL3, CXCL5, CXCL6 and CXCL8 were measured using ELISA (BioTechne for CXCL1, 5, 6, 8, Abcam for CXCL3). CCL26, CXCL2 and CCL2 concentrations were measured by using a customized Bio-Plex Assay (BioRad, Hercules, CA), using special plate reader (Bio-Plex 200 Systems, BioRad) and software (Bio-Plex manager), according to the manufacturer's instruction.

Fibrocyte migration

Fibrocytes precursors were isolated from peripheral blood as described previously (Dupin et al., 2016). Fibrocyte migration was assessed using a modified Boyden chamber assay. The transwell inserts (pore size 8 µm, Dutscher) and the wells were coated for 1h at room temperature with poly-lysine-ethylene glycol (PEG-PLL, SuSoS, Dübendorf, Switzerland) to prevent cell adhesion. A total of 0.3 x 10^6 NANT cells resuspended in 0.2 ml DMEM,

containing 4.5 g/l glucose and L-glutamine, supplemented with penicillin/streptomycin and MEM non-essential amino acid solution were added to the upper compartment of each well. When indicated, NANT cells were pretreated for 30 min at 37°C with 200nM reparixin (MedChem Express), an antagonist of CXCR1-2. Supernatants of tissular $CD8^+$ T cells from non-smoking control subjects or COPD patients were added to the bottom compartment of each well. When indicated, supernatants were pretreated for 30 min at 37°C with blocking Ab against CXCL8 (clone 6217, BioTechne, 1µg/mL) or respective control Ab. After 12h, the content of bottom compartment was removed and DAPI staining was performed to exclude dying cells. Cells were then fixed, permeabilized and stained with anti-Collagen Type I-FITC (Sigma Aldrich), anti-CD45-APC (BD Pharmingen), anti-CXCR1-PE and anti-CXCR2-APC-Cy7 (Miltenyi Biotec, Paris, France). Fibrocyte migration was assessed by flow cytometry using double labeling CD45-Collagen I. To obtain absolute values of migratory cells, flow cytometric counts for each condition were obtained during a constant predetermined time period (1 min). The fraction of migratory fibrocytes was defined as the number $CD45^+$ $Col1^+$ cells counted in the bottom chamber divided by the number of total added cells. These values were normalized to the fraction of migratory fibrocytes obtained in the control condition.

Fibrocyte $CD8^+$ and $CD4^+$ T cell purification

Peripheral blood mononuclear cells (PBMCs) were first separated from the whole blood by Ficoll-Hypaque (Eurobio Scientific, Les Ulis, France) density gradient centrifugation. Cells were washed twice in cold PBS containing 0.5% bovine serum albumin (BSA, Sigma-Aldrich, Saint Quentin-Fallavier, France) and 2 mM Ethylene Diamine Tetra-acetic Acid (EDTA, Invitrogen, Cergy Pontoise, France). $CD8^+$ and $CD4^+$ T cells were purified by positive selecting using CD8 and CD4 microbeads, respectively (Miltenyi Biotech, Paris,

France). $CD8^+/CD4^+$ T cells were washed in a buffered solution ("CTL-Wash™", Cellular Technology Limited, Bonn, Germany) and resuspended in a serum-free freezing media ("CTL-Cryo™ Medium", Cellular Technology Limited, Bonn, Germany) for cryopreservation of freshly-isolated $CD8^+/CD4^+$ T cells during fibrocyte differentiation. The $CD8^+$ or $CD4^+$ T cells-depleted cell fraction was then depleted from $CD3^+$ cells using CD3 microbeads (Miltenyi Biotec). Cell suspension containing fibrocyte precursors was cultured during at least 14 days to induce fibrocyte differentiation: a total of 2.10^6 cells resuspended in 1 ml DMEM (Fisher Scientific, Illkirch, France), containing 4.5 g/l glucose and glutaMAX, supplemented with 20% fetal calf serum (Biowest, Riverside, USA), penicillin/streptomycin and MEM non-essential amino acid solution (Sigma-Aldrich), was added to each well of a 12 well plate. After one week in culture, fibrocyte differentiation was induced by changing the medium for a serum-free medium. Mediums were changed every 2-3 days.

Fibrocyte/$CD8^+$ T cells and fibrocyte/$CD4^+$ T cells co-culture assay

One day before co-culture, $CD8^+$ T or $CD4^+$ cells were thawed. A buffer solution previously heated to 37°C (PBS 1X with 0.5% BSA and 2mM EDTA) was added to the cell suspension. $CD8^+/CD4^+$ T cells were washed with PBS and resuspended in DMEM supplemented with 8% fetal calf serum for a final concentration of $0.5.10^6$ cells/mL. $CD8^+/CD4^+$ T cells were either stimulated with a low dose of CD3 antibody (3µg / 10^6 cells) to promote cell survival without stimulating cell proliferation ("non-activated" condition), or stimulated overnight with anti-CD3/CD28 coated microbeads (Fisher Scientific) with a bead-to-cell ratio of 1:1 ("activated" condition). At day 0 (co-culture), these beads were removed, $CD8^+/CD4^+$ T cells were stained with 5 µM CellTrace Violet (Fisher Scientific) in case of proliferation experiments, before being added to fibrocyte cultures ($0.5.10^6$ $CD8^+/CD4^+$ T cells/well). In

blocking experiments, the antibodies (Abs) directed against LFA-1 (clone HI111, BioLegend, 1µg/mL), CD54 (clone HA58, eBioscience), CD86 (clone IT2.2, eBioscience, 10µg/mL) or CD44 (clone 82102, BioTechne, 10µg/mL) were used with their respective control Abs, mIgG1 κ (clone MOPC-21, BioLegend), mIgG2b κ (eBM 2b, eBioscience), mIgG2B (133303, BioTechne). In LFA-1 and CD44 blocking experiments as well as in glucocorticoid drugs experiments, $CD8^+$ T cells were preincubated respectively with corresponding Abs, budesonide or fluticasone propionate (10^{-8}M, MedChemExpress) at 37°C for 1h before being added to fibrocytes. In CD54 and CD86 blocking experiments, fibrocytes were preincubated with corresponding Abs at 37°C for 1h before adding $CD8^+$ T cells. For indirect co-culture, $CD8^+$ T cells were cultured in 0.4 µm transwell inserts (Sigma-Aldrich) for 12-well plates.

Live imaging

For time-lapse microscopy, cells were imaged after 2 days of co-culture, at 37°C and with 5% CO_2 on an inverted DMi8 stand microscope (Leica, Microsystems, Wetzlar, Germany) equipped with a Flash 4.0 sCMOS camera (Hamamatsu, Japan). The objective used was a HC PL FL L 20X dry 0.4 NA PH1. The multi-positions were done with a ASI MS-2000-500 motorized stage (Applied Scientific Instrumentation, Eugene, USA). The 37°C/5%CO2 atmosphere was created with an incubator box and a gaz heating system (Pecon GmbH, Erbach, Germany). This system was controlled by MetaMorph software (Molecular Devices, Sunnyvale, USA). Phase contrast images were collected every 2 min for 12h. Image analysis and measurements were performed with the ImageJ software. Using the plugin "Cell counter " of the Fiji software, the number of $CD8^+$ T cells in direct contact with a fibrocyte as well as the number of free $CD8^+$ T cells were manually counted at the beginning of the acquisition and after 12 hours of acquisition. Cell tracking was performed

using the “Manual Tracking” plugin of the Fiji software to determine the durations of contacts between tracked $CD8^+$ T cell with fibrocytes and the frequency of contact. A contact was defined manually by a direct interaction between $CD8^+$ T cell and fibrocyte. Five numerical variables were collected to characterize $CD8^+$ T cell dynamic over time. The mean speed corresponded to the track length divided by the time of tracking duration. The mean free speed corresponded the length of the track when the T cell was not interacting with any other cell, divided by the time spent free. The mean contact speed corresponded to the length of the track when the T cell is in contact with a fibrocyte, divided by the time spent in contact. For each T cell and for each contact, a contact time was defined as the time spent in contact until the T cell becomes free again. Then, each T cell can have many contact times with fibrocytes. The contact coefficient was defined by the proportion of time the T cell was in contact with a fibrocyte divided by the time of tracking duration.

$CD8^+$ and $CD4^+$ T cell characterization by flow cytometry

Four or 6 days after co-culture, $CD8^+$/$CD4^+$ T cells were harvested and manually counted before being processed for FACS analysis. Dead cells were excluded by using DAPI or the Zombie NIR fixable viability kit (BioLegend). Intracellular cytokines were assessed following stimulation with PMA (25 ng/ml, Sigma-Aldrich), ionomycin (1µM, Sigma-Aldrich) for 4h and brefeldin A (5µg/ml,Sigma-Aldrich) for the last 3 h. Cells were stained with anti-CD8-PerCP-Vio700 or anti-CD4-PerCP-Vio700, anti-CD45-RA-FITC, and then fixed, permeabilized using the IntraPrep Permeabilization Reagent Kit (Beckman Coulter) and stained with anti-Granzyme-APC, anti-TNF-α-PE, anti-IFN-γ-APC, anti-IL-17- PE-Cy7, anti-IL-10-PE or isotype controls (Miltenyi Biotech, Paris, France). The percentage of cell proliferation was estimated using Cell Trace Violet fluorescence loss. FACS data were acquired using a Canto II 4-Blue 2-Violet 2-Red laser configuration (BD Biosciences). Flow

cytometry analysis were performed using Diva 8 (BD Biosciences). Human TNF-α concentration levels were quantified using ELISA following manufacturer's recommendations (BioTechne). Values below the detection limit were counted as zero.

CD107a expression of CD8$^+$ T cells

Six days after co-culture, CD8$^+$ T cells were harvested and stained to assess CD107a expression following stimulation with PMA (25 ng/ml, Sigma-Aldrich) and ionomycin (1µM, Sigma-Aldrich) for 3h. Cells were stained with anti-CD8-PerCP-Vio700, anti-CD45-RA-FITC or isotype controls (Miltenyi Biotech, Paris, France). For membrane expression analysis, cells were then stained with anti-CD107a-PE or isotype control (BD Biosciences, San Jose, CA). For total expression analysis, cells were fixed, permeabilized using the IntraPrep Permeabilization Reagent Kit (Beckman Coulter) and stained with anti-CD107a-PE or isotype control. FACS data were acquired using a Canto II 4-Blue 2-Violet 2-Red laser configuration (BD Biosciences).

Bronchial epithelial cell culture

Human basal bronchial epithelial cells were derived from bronchial specimens (Table S9) as described previously (Trian et al., 2015). Bronchial epithelial tissue was cultured in PneumaCult™-Ex medium (Stemcell Technologies, Vancouver, Canada) under water-saturated 5% CO_2 atmosphere at 37°C until epithelial cells reached 80-90% confluence. For cytotoxic assay, basal bronchial epithelial cells were plated on 24-wells plate in PneumaCult™-Ex medium.

Cell Trace Violet-based cytotoxic activity of CD8$^+$ T cells

After 6 days of co-culture, $CD8^+$ T cells were resuspended (2.10^6 cells/ml), and labeled with 5 µM Cell Trace Violet (Fisher Scientific) following manufacturer's recommendations. Cell Trace Violet-labeled $CD8^+$ T cells as effector cells and primary basal bronchial epithelial cells as target cells were co-incubated at effector:target ratio of 4:1 in PneumaCult™-Ex medium. After 6 hours, $CD8^+$ T cells were kept with supernatant, and basal epithelial cells were harvested by using 0,05% trypsin-EDTA (Fisher Scientific). The entire content of each well was stained using Annexin V- Propidium iodide (Fisher Scientific) for the detection of apoptotic and living cells by flow cytometry, according to the manufacturer's instructions. $CD8^+$ T cells exclusion was performed based on the Cell Trace Violet-based fluorescence performed 6 hours before.

Label-free quantitative proteomics

4 independent biological replicates on total protein extracts from fibrocytes cultured alone (control condition), or co-cultured with $CD8^+$ T cells that have been previously non-activated or activated during 6 days. 10 µg of proteins were loaded on a 10% acrylamide SDS-PAGE gel and proteins were visualized by Colloidal Blue staining. Migration was stopped when samples had just entered the resolving gel and the unresolved region of the gel was cut into only one segment. Each SDS-PAGE band was cut into 1 mm x 1 mm gel pieces. Gel pieces were destained in 25 mM ammonium bicarbonate (NH_4HCO_3), 50% Acetonitrile (ACN) and shrunk in ACN for 10 min. After ACN removal, gel pieces were dried at room temperature. Proteins were first reduced in 10 mM dithiothreitol, 100 mM NH_4HCO_3 for 60 min at 56°C then alkylated in 100 mM iodoacetamide, 100 mM NH_4HCO_3 for 60 min at room temperature and shrunk in ACN for 10 min. After ACN removal, gel pieces were rehydrated with 50 mM NH_4HCO_3 for 10 min at room temperature. Before protein digestion, gel pieces were shrunk in ACN for 10 min and dried at room temperature.

Proteins were digested by incubating each gel slice with 10 ng/µl of trypsin (V5111, Promega) in 40 mM NH_4HCO_3, rehydrated at 4°C for 10 min, and finally incubated overnight at 37°C. The resulting peptides were extracted from the gel by three steps: a first incubation in 40 mM NH_4HCO_3 for 15 min at room temperature and two incubations in 47.5% ACN, 5% formic acid for 15 min at room temperature. The three collected extractions were pooled with the initial digestion supernatant, dried in a SpeedVac, and resuspended with 0.1% formic acid for a final concentration of 0.02 µg/µL. NanoLC-MS/MS analysis were performed using an Ultimate 3000 RSLC Nano-UPHLC system (Thermo Scientific, USA) coupled to a nanospray Orbitrap Fusion™ Lumos™ Tribrid™ Mass Spectrometer (Thermo Fisher Scientific, California, USA). Each peptide extracts were loaded on a 300 µm ID x 5 mm PepMap C_{18} precolumn (Thermo Scientific, USA) at a flow rate of 10 µL/min. After a 3 min desalting step, peptides were separated on a 50 cm EasySpray column (75 µm ID, 2 µm C_{18} beads, 100 Å pore size, ES903, Thermo Fisher Scientific) with a 4-40% linear gradient of solvent B (0.1% formic acid in 80% ACN) in 115 min. The separation flow rate was set at 300 nL/min. The mass spectrometer operated in positive ion mode at a 1.9 kV needle voltage. Data were acquired using Xcalibur 4.4 software in a data-dependent mode. MS scans (m/z 375-1500) were recorded at a resolution of R = 120000 (@ m/z 200), a standard AGC target and an injection time in automatic mode, followed by a top speed duty cycle of up to 3 seconds for MS/MS acquisition. Precursor ions (2 to 7 charge states) were isolated in the quadrupole with a mass window of 1.6 Th and fragmented with HCD@28% normalized collision energy. MS/MS data were acquired in the Orbitrap cell with a resolution of R=30000 (@m/z 200), a standard AGC target and a maximum injection time in automatic mode. Selected precursors were excluded for 60 seconds. Protein identification and Label-Free Quantification (LFQ) were done in Proteome Discoverer 2.5. MS Amanda 2.0, Sequest HT and Mascot 2.5 algorithms were used for protein identification

in batch mode by searching against a Uniprot Homo sapiens database (81 856 entries, release January 20th, 2023). Two missed enzyme cleavages were allowed for the trypsin. Mass tolerances in MS and MS/MS were set to 10 ppm and 0.02 Da. Oxidation (M) and acetylation (K) were searched as dynamic modifications and carbamidomethylation (C) as static modification. Peptide validation was performed using Percolator algorithm and only "high confidence" peptides were retained corresponding to a 1% false discovery rate at peptide level (Käll et al., 2007). Minora feature detector node (LFQ) was used along with the feature mapper and precursor ions quantifier. The normalization parameters were selected as follows: 1: Unique peptides, 2: Precursor abundance based on intensity, 3: Normalization mode: total peptide amount, 4: Protein abundance calculation: summed abundances, 5: Protein ratio calculation : pairwise ratio based, 6: Imputation mode : Low abundance resampling and 7: Hypothesis test : t-test (background based). Quantitative data were considered for master proteins, quantified by a minimum of 2 unique peptides, a fold changes above 2 and a statistical p-value adjusted using Benjamini-Hochberg correction for the FDR lower than 0.05. The mass spectrometry proteomics data have been deposited to the ProteomeXchange Consortium via the PRIDE (Deutsch et al., 2020) partner repository with the dataset identifier PXD041402. Proteins were clusterized according to their functions by using the Kyoto Encyclopedia of genes and genome analysis in the search tool for retrieval of interaction between genes and proteins (STRING) database. More global analysis of the data was performed via use of Ingenuity Pathway Analysis (IPA; Qiagen). We used the 'Core Analysis' package to identify relationships, mechanisms, functions, and pathways relevant to a dataset.

The mathematical model

Exhaustive description of the mathematical model is provided in the supplementary text.

To understand the interaction between fibrocyte and $CD8^+$ T cells in the spatial cellular organization in the peribronchial area, we constructed a discrete time cellular automata model. Two agent types are introduced - $CD8^+$ T cell agents and fibrocytes agents, denoted C and F respectively. C and F cells evolve on a lattice in two-dimensions. We take as surface of interest a zone with a crown shape, containing 3 652 lattice sites corresponding to a total area of approximately 179 000 μm^2, which is in agreement with our in *situ* measurements. Reflecting (zero-flux) boundary conditions are imposed at the external and internal borders. On each site, there is at most one cell. The lattice is initially randomly seeded with both F and C cells at densities corresponding at the mean distribution of non-smokers subjects, reflecting the "healthy" situation : $n_0(C)$ = 660 cells/mm^2, and $n_0(F)$ = 106 cells/mm^2. This corresponds to an average value of $N_0(C)$ =118 C cells and $N_0(F)$ =19 F cells.

We assumed that for a healthy subject as for a patient with COPD, the same model can be applied but with different parameters. These parameters are estimated thanks to experiments and data from the literature (see supplementary text and (Dupin, Eyraud, et al., 2023) for a complete description, Table S11 for numerical values).

The notations and parameters of the mathematical model are summarized in Table S10 and their numerical values are given in Table S11. We now describe the behavior of the cells and their interactions. F and C cells infiltrate into the peribronchial area at the stable state with the respective probabilities p_{istaF} and p_{istaC}, and during exacerbation, a supplementary infiltration can occur, each year, with the probability p_{iexaF} (resp. p_{iexaC}). In the model, C cells can proliferate with a very low probability p_C, but the presence of F cells in the local neighbourhood of a C cell can induce C cell division with increased probability $p_{C/F}$, based on our own results and another study (Afroj et al., 2021). We suppose that fibrocytes do not proliferate, as shown by our own *in vitro* observations (data not shown) and other studies (Ling et al., 2019; Schmidt et al., 2003). F and C cells can move, with probabilities which

are determined by the results from chemotaxis experiments (Figure 2). F and C cells die with a "basal" probability p_{dC} (respectively p_{dF}). C cells also die with an increased probability p_{dC+} when the considered C cell has many other C cells in its neighbourhood, in agreement with previous data (Zenke et al., 2020). Some of the probabilities are independent of the local environment (p_{istaF}, p_{istaC}, p_{iexaF}, p_{iexaC}, p_C), the other ones being dependent of the local environment ($p_{C/F,}$, p_{dC+} and displacement probabilities) (Figure 8A).

Each simulation represents a total duration of 20 years and is divided into 3 504 000 iterations, of 3 minutes each. Each type of simulation is performed 160 times. This time period allowed the investigation of COPD development. At the final state (20 years), the total numbers of F and C cells, the densities of C cells in interaction with F cells, the minimal distances between C and F cells, and the number and composition of clusters were quantified in the control and COPD situations. For therapeutic interventions, different dynamics were applied during 7 years, starting from COPD states that have been generated using the application of a COPD dynamics during 20 years. At the final state (7 years after the application of therapeutic dynamics), the same outcomes than at 20 years were quantified.

Definition of biological and technical replicates

Biological replicates are samples purified from different patients. Technical replicates are repeated measurements in the same biological samples. For *in situ* analyses, both technical replicates (measurements performed on at least 2 bronchi) and biological replicates have been performed. For most of *in vitro* analyses, only biological replicates have been obtained, because our cells of interest have a very limited lifespan in culture and experiments can therefore be performed only once. Exceptions include migration assays and ELISA

measurements, with both technical duplicates and biological replicates. For simulations, technical replicates have been performed, with each type of simulation being repeated 160 times.

Statistical analyses

Statistical significance, defined as $P < 0.05$, was analyzed by t-tests and MANOVA for variables with parametric distribution, and by Kruskal-Wallis with multiple comparison z tests, Mann-Whitney tests, Wilcoxon tests and Spearman correlation coefficients for variables with non-parametric distribution and by two-way ANOVA for distribution tests, using Graphpad Prism 6 software. RStudio software was used to perform stepwise regression and multivariate regression analyses.

References

Abe, R., Donnelly, S. C., Peng, T., Bucala, R., & Metz, C. N. (2001). Peripheral Blood Fibrocytes : Differentiation Pathway and Migration to Wound Sites1. *The Journal of Immunology*, *166*(12), 7556-7562. https://doi.org/10.4049/jimmunol.166.12.7556

Afroj, T., Mitsuhashi, A., Ogino, H., Saijo, A., Otsuka, K., Yoneda, H., Tobiume, M., Nguyen, N. T., Goto, H., Koyama, K., Sugimoto, M., Kondoh, O., Nokihara, H., & Nishioka, Y. (2021). Blockade of PD-1/PD-L1 Pathway Enhances the Antigen-Presenting Capacity of Fibrocytes. *The Journal of Immunology*, *206*(6), 1204-1214. https://doi.org/10.4049/jimmunol.2000909

Araki, K., Youngblood, B., & Ahmed, R. (2010). The role of mTOR in memory CD8+ T-cell differentiation. *Immunological reviews*, *235*(1), 234-243. https://doi.org/10.1111/j.0105-2896.2010.00898.x

Backer, R. A., Hombrink, P., Helbig, C., & Amsen, D. (2018). The Fate Choice Between Effector and Memory T Cell Lineages : Asymmetry, Signal Integration, and Feedback to Create Bistability. *Advances in Immunology*, *137*, 43-82. https://doi.org/10.1016/bs.ai.2017.12.003

Balmelli, C., Ruggli, N., McCullough, K., & Summerfield, A. (2005). Fibrocytes are potent stimulators of anti-virus cytotoxic T cells. *Journal of Leukocyte Biology*, *77*(6), 923-933. https://doi.org/10.1189/jlb.1204701

Barnes, P. J. (2016). Inflammatory mechanisms in patients with chronic obstructive pulmonary disease. *The Journal of Allergy and Clinical Immunology*, *138*(1), 16-27. https://doi.org/10.1016/j.jaci.2016.05.011

Bertini, R., Allegretti, M., Bizzarri, C., Moriconi, A., Locati, M., Zampella, G., Cervellera, M. N., Di Cioccio, V., Cesta, M. C., Galliera, E., Martinez, F. O., Di Bitondo, R., Troiani, G., Sabbatini, V., D'Anniballe, G., Anacardio, R., Cutrin, J. C., Cavalieri, B., Mainiero, F., …

Colotta, F. (2004). Noncompetitive allosteric inhibitors of the inflammatory chemokine receptors CXCR1 and CXCR2 : Prevention of reperfusion injury. *Proceedings of the National Academy of Sciences of the United States of America*, *101*(32), 11791-11796. https://doi.org/10.1073/pnas.0402090101

Bianchetti, L., Barczyk, M., Cardoso, J., Schmidt, M., Bellini, A., & Mattoli, S. (2012). Extracellular matrix remodelling properties of human fibrocytes. *Journal of Cellular and Molecular Medicine*, *16*(3), 483-495. https://doi.org/10.1111/j.1582-4934.2011.01344.x

Bivas-Benita, M., Gillard, G. O., Bar, L., White, K. A., Webby, R. J., Hovav, A.-H., & Letvin, N. L. (2013). Airway CD8 + T cells induced by pulmonary DNA immunization mediate protective anti-viral immunity. *Mucosal Immunology*, *6*(1), Article 1. https://doi.org/10.1038/mi.2012.59

Bucala, R. J. (2022). Targeting fibrocytes in autoimmunity. *Proceedings of the National Academy of Sciences*, *119*(5), e2121739119. https://doi.org/10.1073/pnas.2121739119

Bucala, R., Spiegel, L. A., Chesney, J., Hogan, M., & Cerami, A. (1994). Circulating fibrocytes define a new leukocyte subpopulation that mediates tissue repair. *Molecular Medicine (Cambridge, Mass.)*, *1*(1), 71-81.

Chang, J. T., Palanivel, V. R., Kinjyo, I., Schambach, F., Intlekofer, A. M., Banerjee, A., Longworth, S. A., Vinup, K. E., Mrass, P., Oliaro, J., Killeen, N., Orange, J. S., Russell, S. M., Weninger, W., & Reiner, S. L. (2007). Asymmetric T lymphocyte division in the initiation of adaptive immune responses. *Science (New York, N.Y.)*, *315*(5819), 1687-1691. https://doi.org/10.1126/science.1139393

Chang, Y., Nadigel, J., Boulais, N., Bourbeau, J., Maltais, F., Eidelman, D. H., & Hamid, Q. (2011). CD8 positive T cells express IL-17 in patients with chronic obstructive pulmonary disease. *Respiratory Research*, *12*(1), 43. https://doi.org/10.1186/1465-9921-12-43

Chesney, J., Bacher, M., Bender, A., & Bucala, R. (1997). The peripheral blood fibrocyte is a potent antigen-presenting cell capable of priming naive T cells in situ. *Proceedings of the National Academy of Sciences*, *94*(12), 6307-6312. https://doi.org/10.1073/pnas.94.12.6307

Chrysofakis, G., Tzanakis, N., Kyriakoy, D., Tsoumakidou, M., Tsiligianni, I., Klimathianaki, M., & Siafakas, N. M. (2004). Perforin expression and cytotoxic activity of sputum CD8+ lymphocytes in patients with COPD. *Chest*, *125*(1), 71-76. https://doi.org/10.1378/chest.125.1.71

Conlon, T. M., John-Schuster, G., Heide, D., Pfister, D., Lehmann, M., Hu, Y., Ertüz, Z., Lopez, M. A., Ansari, M., Strunz, M., Mayr, C., Angelidis, I., Ciminieri, C., Costa, R., Kohlhepp, M. S., Guillot, A., Günes, G., Jeridi, A., Funk, M. C., … Yildirim, A. Ö. (2020). Inhibition of LTβR signalling activates WNT-induced regeneration in lung. *Nature*, *588*(7836), 151-156. https://doi.org/10.1038/s41586-020-2882-8

Dayer, J.-M. (2003). How T-lymphocytes are activated and become activators by cell-cell interaction. *European Respiratory Journal*, *22*(44 suppl), 10s-15s. https://doi.org/10.1183/09031936.03.00000403b

Deutsch, E. W., Bandeira, N., Sharma, V., Perez-Riverol, Y., Carver, J. J., Kundu, D. J., García-Seisdedos, D., Jarnuczak, A. F., Hewapathirana, S., Pullman, B. S., Wertz, J., Sun, Z., Kawano, S., Okuda, S., Watanabe, Y., Hermjakob, H., MacLean, B., MacCoss, M. J., Zhu, Y., … Vizcaíno, J. A. (2020). The ProteomeXchange consortium in 2020 : Enabling « big data » approaches in proteomics. *Nucleic Acids Research*, *48*(D1), D1145-D1152. https://doi.org/10.1093/nar/gkz984

Douglas, R. S., Kahaly, G. J., Patel, A., Sile, S., Thompson, E. H. Z., Perdok, R., Fleming, J. C., Fowler, B. T., Marcocci, C., Marinò, M., Antonelli, A., Dailey, R., Harris, G. J., Eckstein, A., Schiffman, J., Tang, R., Nelson, C., Salvi, M., Wester, S., … Smith, T. J. (2020). Teprotumumab for the Treatment of Active Thyroid Eye Disease. *The New England Journal of Medicine*, *382*(4), 341-352. https://doi.org/10.1056/NEJMoa1910434

Dupin, I., Allard, B., Ozier, A., Maurat, E., Ousova, O., Delbrel, E., Trian, T., Bui, H.-N., Dromer, C., Guisset, O., Blanchard, E., Hilbert, G., Vargas, F., Thumerel, M., Marthan, R., Girodet, P.-O., & Berger, P. (2016). Blood fibrocytes are recruited during acute exacerbations of chronic obstructive pulmonary disease through a CXCR4-dependent pathway. *The Journal of Allergy and Clinical Immunology*, *137*(4), Article 4. https://doi.org/10.1016/j.jaci.2015.08.043

Dupin, I., Contin-Bordes, C., & Berger, P. (2018). Fibrocytes in Asthma and Chronic Obstructive Pulmonary Disease : Variations on the Same Theme. *American Journal of Respiratory Cell and Molecular Biology*, *58*(3), Article 3. https://doi.org/10.1165/rcmb.2017-0301PS

Dupin, I., Eyraud, E., Maurat, É., Sac-Épée, J.-M., & Vallois, P. (2023). Probabilistic cellular automata modelling of intercellular interactions in airways : Complex pattern formation in patients with chronic obstructive pulmonary disease. *Journal of Theoretical Biology*, *564*, 111448. https://doi.org/10.1016/j.jtbi.2023.111448

Dupin, I., Henrot, P., Maurat, E., Abohalaka, R., Chaigne, S., Hamrani, D. E., Eyraud, E., Prevel, R., Esteves, P., Campagnac, M., Dubreuil, M., Cardouat, G., Bouchet, C., Ousova, O., Dupuy, J.-W., Trian, T., Thumerel, M., Begueret, H., Girodet, P.-O., … Berger, P. (2023). *CXCR4 blockade alleviates pulmonary and cardiac outcomes in early COPD* (p. 2023.03.10.529743). bioRxiv. https://doi.org/10.1101/2023.03.10.529743

Dupin, I., Thumerel, M., Maurat, E., Coste, F., Eyraud, E., Begueret, H., Trian, T., Montaudon, M., Marthan, R., Girodet, P.-O., & Berger, P. (2019). Fibrocyte accumulation in the airway walls of COPD patients. *The European Respiratory Journal*, *54*(3), Article 3. https://doi.org/10.1183/13993003.02173-2018

Dustin, M. L. (2008). T-cell activation through immunological synapses and kinapses. *Immunological Reviews*, *221*, 77-89. https://doi.org/10.1111/j.1600-065X.2008.00589.x

Ely, K. H., Cookenham, T., Roberts, A. D., & Woodland, D. L. (2006). Memory T cell populations in the lung airways are maintained by continual recruitment. *Journal of Immunology (Baltimore, Md.: 1950)*, *176*(1), 537-543. https://doi.org/10.4049/jimmunol.176.1.537

Fernando, R., Atkins, S., Raychaudhuri, N., Lu, Y., Li, B., Douglas, R. S., & Smith, T. J. (2012). Human fibrocytes coexpress thyroglobulin and thyrotropin receptor. *Proceedings of the National Academy of Sciences*, *109*(19), 7427-7432. https://doi.org/10.1073/pnas.1202064109

Fernando, R., Caldera, O., & Smith, T. J. (2021). Therapeutic IGF-I receptor inhibition alters fibrocyte immune phenotype in thyroid-associated ophthalmopathy. *Proceedings of the National Academy of Sciences*, *118*(52), e2114244118. https://doi.org/10.1073/pnas.2114244118

Freeman, C. M., Curtis, J. L., & Chensue, S. W. (2007). CC chemokine receptor 5 and CXC chemokine receptor 6 expression by lung CD8+ cells correlates with chronic obstructive pulmonary disease severity. *The American Journal of Pathology*, *171*(3), 767-776. https://doi.org/10.2353/ajpath.2007.061177

Freeman, C. M., Han, M. K., Martinez, F. J., Murray, S., Liu, L. X., Chensue, S. W., Polak, T. J., Sonstein, J., Todt, J. C., Ames, T. M., Arenberg, D. A., Meldrum, C. A., Getty, C., McCloskey, L., & Curtis, J. L. (2010). Cytotoxic potential of lung CD8+ T cells increases with COPD severity and with in vitro stimulation by IL-18 or IL-15. *Journal of immunology (Baltimore, Md. : 1950)*, *184*(11), 6504-6513. https://doi.org/10.4049/jimmunol.1000006

Gillen, J. R., Zhao, Y., Harris, D. A., LaPar, D. J., Stone, M. L., Fernandez, L. G., Kron, I. L., & Lau, C. L. (2013). Rapamycin Blocks Fibrocyte Migration and Attenuates Bronchiolitis Obliterans in a Murine Model. *The Annals of thoracic surgery*, *95*(5), 1768-1775. https://doi.org/10.1016/j.athoracsur.2013.02.021

Global Initiative for Chronic Obstructive Lung Disease. (s. d.). Global Initiative for Chronic Obstructive Lung Disease - GOLD. Consulté 6 février 2023, à l'adresse https://goldcopd.org/

Gribben, J. G., Freeman, G. J., Boussiotis, V. A., Rennert, P., Jellis, C. L., Greenfield, E., Barber, M., Restivo, V. A., Ke, X., & Gray, G. S. (1995). CTLA4 mediates antigen-specific apoptosis of human T cells. *Proceedings of the National Academy of Sciences*, *92*(3), 811-815. https://doi.org/10.1073/pnas.92.3.811

Grundy, S., Plumb, J., Lea, S., Kaur, M., Ray, D., & Singh, D. (2013). Down regulation of T cell receptor expression in COPD pulmonary CD8 cells. *PloS One*, *8*(8), e71629. https://doi.org/10.1371/journal.pone.0071629

Hayashi, H., Kawakita, A., Okazaki, S., Yasutomi, M., Murai, H., & Ohshima, Y. (2013). IL-17A/F modulates fibrocyte functions in cooperation with CD40-mediated signaling. *Inflammation*, *36*(4), 830-838. https://doi.org/10.1007/s10753-013-9609-z

Henrot, P., Beaufils, F., Thumerel, M., Eyraud, E., Boudoussier, A., Begueret, H., Maurat, E., Girodet, P.-O., Marthan, R., Berger, P., Dupin, I., & Zysman, M. (2021). Circulating fibrocytes as a new tool to predict lung cancer progression after surgery? *The European Respiratory Journal*, 2101221. https://doi.org/10.1183/13993003.01221-2021

Henrot, P., Eyraud, E., Maurat, E., Point, S., Cardouat, G., Quignard, J.-F., Esteves, P., Trian, T., Girodet, P.-O., Marthan, R., Zysman, M., Berger, P., & Dupin, I. (2022). Muscarinic receptor M3 activation promotes fibrocytes contraction. *Frontiers in Pharmacology*, *13*. https://www.frontiersin.org/articles/10.3389/fphar.2022.939780

Henrot, P., Prevel, R., Berger, P., & Dupin, I. (2019). Chemokines in COPD : From Implication to Therapeutic Use. *International Journal of Molecular Sciences*, *20*(11), Article 11. https://doi.org/10.3390/ijms20112785

Hodge, G., Nairn, J., Holmes, M., Reynolds, P. N., & Hodge, S. (2007). Increased intracellular T helper 1 proinflammatory cytokine production in peripheral blood, bronchoalveolar lavage and intraepithelial T cells of COPD subjects. *Clinical and Experimental Immunology*, *150*(1), 22-29. https://doi.org/10.1111/j.1365-2249.2007.03451.x

Hogg, J. C., Chu, F., Utokaparch, S., Woods, R., Elliott, W. M., Buzatu, L., Cherniack, R. M., Rogers, R. M., Sciurba, F. C., Coxson, H. O., & Paré, P. D. (2004). The nature of small-airway obstruction in chronic obstructive pulmonary disease. *The New England Journal of Medicine*, *350*(26), 2645-2653. https://doi.org/10.1056/NEJMoa032158

Hogg, J. C., Williams, J., Richardson, J. B., Macklem, P. T., & Thurlbeck, W. M. (1970). Age as a Factor in the Distribution of Lower-Airway Conductance and in the Pathologic Anatomy of Obstructive Lung Disease. *New England Journal of Medicine*, *282*(23), 1283-1287. https://doi.org/10.1056/NEJM197006042822302

Hombrink, P., Helbig, C., Backer, R. A., Piet, B., Oja, A. E., Stark, R., Brasser, G., Jongejan, A., Jonkers, R. E., Nota, B., Basak, O., Clevers, H. C., Moerland, P. D., Amsen, D., & van Lier, R. A. W. (2016). Programs for the persistence, vigilance and control of human CD8+ lung-resident memory T cells. *Nature Immunology*, *17*(12), 1467-1478. https://doi.org/10.1038/ni.3589

Hufford, M. M., Kim, T. S., Sun, J., & Braciale, T. J. (2011). Antiviral CD8+ T cell effector activities in situ are regulated by target cell type. *The Journal of Experimental Medicine*, *208*(1), 167-180. https://doi.org/10.1084/jem.20101850

Hurst, J. R., Vestbo, J., Anzueto, A., Locantore, N., Müllerova, H., Tal-Singer, R., Miller, B., Lomas, D. A., Agusti, A., Macnee, W., Calverley, P., Rennard, S., Wouters, E. F. M., Wedzicha, J. A., & Evaluation of COPD Longitudinally to Identify Predictive Surrogate Endpoints (ECLIPSE) Investigators. (2010). Susceptibility to exacerbation in chronic obstructive pulmonary disease. *The New England Journal of Medicine*, *363*(12), 1128-1138. https://doi.org/10.1056/NEJMoa0909883

Käll, L., Canterbury, J. D., Weston, J., Noble, W. S., & MacCoss, M. J. (2007). Semi-supervised learning for peptide identification from shotgun proteomics datasets. *Nature Methods*, *4*(11), Article 11. https://doi.org/10.1038/nmeth1113

Kaur, M., Smyth, L. J., Cadden, P., Grundy, S., Ray, D., Plumb, J., & Singh, D. (2012). T lymphocyte insensitivity to corticosteroids in chronic obstructive pulmonary disease. *Respiratory Research*, *13*, 20. https://doi.org/10.1186/1465-9921-13-20

Lethbridge, M. W., Kemeny, D. M., Ratoff, J. C., O'Connor, B. J., Hawrylowicz, C. M., & Corrigan, C. J. (2010). A novel technique to explore the functions of bronchial mucosal T cells in chronic obstructive pulmonary disease : Application to cytotoxicity and cytokine immunoreactivity. *Clinical and Experimental Immunology*, *161*(3), 560-569. https://doi.org/10.1111/j.1365-2249.2010.04198.x

Ling, C., Nishimoto, K., Rolfs, Z., Smith, L. M., Frey, B. L., & Welham, N. V. (2019). Differentiated fibrocytes assume a functional mesenchymal phenotype with regenerative potential. *Science Advances*, *5*(5), eaav7384. https://doi.org/10.1126/sciadv.aav7384

Løkke, A., Lange, P., Scharling, H., Fabricius, P., & Vestbo, J. (2006). Developing COPD : A 25 year follow up study of the general population. *Thorax*, *61*(11), 935-939. https://doi.org/10.1136/thx.2006.062802

Lundblad, L. K. A., Thompson-Figueroa, J., Leclair, T., Sullivan, M. J., Poynter, M. E., Irvin, C. G., & Bates, J. H. T. (2005). Tumor Necrosis Factor–α Overexpression in Lung Disease. *American Journal of Respiratory and Critical Care Medicine*, *171*(12), 1363-1370. https://doi.org/10.1164/rccm.200410-1349OC

Mackay, C. R. (2001). Chemokines : Immunology's high impact factors. *Nature Immunology*, *2*(2), 95-101. https://doi.org/10.1038/84298

Maeno, T., Houghton, A. M., Quintero, P. A., Grumelli, S., Owen, C. A., & Shapiro, S. D. (2007). CD8+ T Cells are required for inflammation and destruction in cigarette smoke-induced emphysema in mice. *Journal of Immunology (Baltimore, Md.: 1950)*, *178*(12), 8090-8096. https://doi.org/10.4049/jimmunol.178.12.8090

Manjarres, D. C. G., Axell-House, D. B., Patel, D. C., Odackal, J., Yu, V., Burdick, M. D., & Mehrad, B. (2023). Sirolimus suppresses circulating fibrocytes in idiopathic pulmonary fibrosis in a randomized controlled crossover trial. *JCI Insight*. https://doi.org/10.1172/jci.insight.166901

Mannino, D. M., & Buist, A. S. (2007). Global burden of COPD : Risk factors, prevalence, and future trends. *Lancet (London, England)*, *370*(9589), 765-773. https://doi.org/10.1016/S0140-6736(07)61380-4

McKendry, R. T., Spalluto, C. M., Burke, H., Nicholas, B., Cellura, D., Al-Shamkhani, A., Staples, K. J., & Wilkinson, T. M. A. (2016). Dysregulation of Antiviral Function of CD8+ T Cells in the Chronic Obstructive Pulmonary Disease Lung. Role of the PD-1–PD-L1 Axis. *American Journal of Respiratory and Critical Care Medicine*, *193*(6), 642-651. https://doi.org/10.1164/rccm.201504-0782OC

McMaster, S. R., Wilson, J. J., Wang, H., & Kohlmeier, J. E. (2015). Airway-Resident Memory CD8 T Cells Provide Antigen-Specific Protection against Respiratory Virus Challenge through Rapid IFN-γ Production. *Journal of Immunology (Baltimore, Md.: 1950)*, *195*(1), 203-209. https://doi.org/10.4049/jimmunol.1402975

Mead, J. (1970). The Lung's Quiet Zone. *New England Journal of Medicine*, *282*(23), 1318-1319. https://doi.org/10.1056/NEJM197006042822311

Mehrad, B., Burdick, M. D., & Strieter, R. M. (2009). Fibrocyte CXCR4 regulation as a therapeutic target in pulmonary fibrosis. *The International Journal of Biochemistry & Cell Biology*, *41*(8-9), 1708-1718. https://doi.org/10.1016/j.biocel.2009.02.020

Miller, M. J., Hejazi, A. S., Wei, S. H., Cahalan, M. D., & Parker, I. (2004). T cell repertoire scanning is promoted by dynamic dendritic cell behavior and random T cell motility in the

lymph node. *Proceedings of the National Academy of Sciences of the United States of America*, *101*(4), 998-1003. https://doi.org/10.1073/pnas.0306407101

Mitsuhashi, A., Koyama, K., Ogino, H., Afroj, T., Nguyen, N. T., Yoneda, H., Otsuka, K., Sugimoto, M., Kondoh, O., Nokihara, H., Hanibuchi, M., Takizawa, H., Shinohara, T., & Nishioka, Y. (2023). Identification of fibrocyte cluster in tumors reveals the role in antitumor immunity by PD-L1 blockade. *Cell Reports*, 112162. https://doi.org/10.1016/j.celrep.2023.112162

Moreau, H. D., Lemaître, F., Terriac, E., Azar, G., Piel, M., Lennon-Dumenil, A.-M., & Bousso, P. (2012). Dynamic in situ cytometry uncovers T cell receptor signaling during immunological synapses and kinapses in vivo. *Immunity*, *37*(2), 351-363. https://doi.org/10.1016/j.immuni.2012.05.014

Morissette, M. C., Parent, J., & Milot, J. (2007). Perforin, granzyme B, and FasL expression by peripheral blood T lymphocytes in emphysema. *Respiratory Research*, *8*(1), 62. https://doi.org/10.1186/1465-9921-8-62

Mrass, P., Oruganti, S. R., Fricke, G. M., Tafoya, J., Byrum, J. R., Yang, L., Hamilton, S. L., Miller, M. J., Moses, M. E., & Cannon, J. L. (2017). ROCK regulates the intermittent mode of interstitial T cell migration in inflamed lungs. *Nature Communications*, *8*(1), 1010. https://doi.org/10.1038/s41467-017-01032-2

Mukhopadhyay, S., Hoidal, J. R., & Mukherjee, T. K. (2006). Role of TNFalpha in pulmonary pathophysiology. *Respiratory Research*, *7*, 125. https://doi.org/10.1186/1465-9921-7-125

Nemzek, J. A., Fry, C., & Moore, B. B. (2013). Adoptive transfer of fibrocytes enhances splenic T-cell numbers and survival in septic peritonitis. *Shock (Augusta, Ga.)*, *40*(2), 106-114. https://doi.org/10.1097/SHK.0b013e31829c3c68

Ngo, V. N., Tang, H. L., & Cyster, J. G. (1998). Epstein-Barr virus-induced molecule 1 ligand chemokine is expressed by dendritic cells in lymphoid tissues and strongly attracts naive T cells and activated B cells. *The Journal of Experimental Medicine*, *188*(1), 181-191. https://doi.org/10.1084/jem.188.1.181

Niedermeier, M., Reich, B., Rodriguez Gomez, M., Denzel, A., Schmidbauer, K., Göbel, N., Talke, Y., Schweda, F., & Mack, M. (2009). CD4+ T cells control the differentiation of Gr1+ monocytes into fibrocytes. *Proceedings of the National Academy of Sciences of the United States of America*, *106*(42), 17892-17897. https://doi.org/10.1073/pnas.0906070106

Obst, R. (2015). The Timing of T Cell Priming and Cycling. *Frontiers in Immunology*, *6*. https://www.frontiersin.org/article/10.3389/fimmu.2015.00563

O'Shaughnessy, T. C., Ansari, T. W., Barnes, N. C., & Jeffery, P. K. (1997). Inflammation in bronchial biopsies of subjects with chronic bronchitis : Inverse relationship of CD8+ T lymphocytes with FEV1. *American Journal of Respiratory and Critical Care Medicine*, *155*(3), 852-857. https://doi.org/10.1164/ajrccm.155.3.9117016

Pilling, D., Zheng, Z., Vakil, V., & Gomer, R. H. (2014). Fibroblasts secrete Slit2 to inhibit fibrocyte differentiation and fibrosis. *Proceedings of the National Academy of Sciences*, *111*(51), 18291-18296. https://doi.org/10.1073/pnas.1417426112

Pombo-Suarez, M., & Gomez-Reino, J. J. (2019). Abatacept for the treatment of rheumatoid arthritis. *Expert Review of Clinical Immunology*, *15*(4), 319-326. https://doi.org/10.1080/1744666X.2019.1579642

Pothen, J. J., Poynter, M. E., & Bates, J. H. T. (2015). A computational model of unresolved allergic inflammation in chronic asthma. *American Journal of Physiology - Lung Cellular and Molecular Physiology*, *308*(4), L384-L390. https://doi.org/10.1152/ajplung.00268.2014

Roos-Engstrand, E., Ekstrand-Hammarström, B., Pourazar, J., Behndig, A. F., Bucht, A., & Blomberg, A. (2009). Influence of smoking cessation on airway T lymphocyte subsets in COPD. *COPD*, *6*(2), 112-120. https://doi.org/10.1080/15412550902755358

Rozelle, A. L., & Genovese, M. C. (2007). Efficacy results from pivotal clinical trials with abatacept. *Clinical and Experimental Rheumatology*, *25*(5 Suppl 46), S30-34.

Saetta, M., Baraldo, S., Corbino, L., Turato, G., Braccioni, F., Rea, F., Cavallesco, G., Tropeano, G., Mapp, C. E., Maestrelli, P., Ciaccia, A., & Fabbri, L. M. (1999). CD8+ve cells in the lungs of smokers with chronic obstructive pulmonary disease. *American Journal of Respiratory and Critical Care Medicine*, *160*(2), 711-717. https://doi.org/10.1164/ajrccm.160.2.9812020

Saetta, M., Di STEFANO, A., Turato, G., Facchini, F. M., Corbino, L., Mapp, C. E., Maestrelli, P., Ciaccia, A., & Fabbri, L. M. (1998). CD8+ T-Lymphocytes in Peripheral Airways of Smokers with Chronic Obstructive Pulmonary Disease. *American Journal of Respiratory and Critical Care Medicine*, *157*(3), 822-826. https://doi.org/10.1164/ajrccm.157.3.9709027

Saunders, R., Kaul, H., Berair, R., Gonem, S., Singapuri, A., Sutcliffe, A. J., Chachi, L., Biddle, M. S., Kaur, D., Bourne, M., Pavord, I. D., Wardlaw, A. J., Siddiqui, S. H., Kay, R. A., Brook, B. S., Smallwood, R. H., & Brightling, C. E. (2019). DP2 antagonism reduces airway smooth muscle mass in asthma by decreasing eosinophilia and myofibroblast recruitment. *Science Translational Medicine*, *11*(479), Article 479. https://doi.org/10.1126/scitranslmed.aao6451

Scheipers, P., & Reiser, H. (1998). Fas-independent death of activated CD4+ T lymphocytes induced by CTLA-4 crosslinking. *Proceedings of the National Academy of Sciences*, *95*(17), 10083-10088. https://doi.org/10.1073/pnas.95.17.10083

Schmidt, M., Sun, G., Stacey, M. A., Mori, L., & Mattoli, S. (2003). Identification of circulating fibrocytes as precursors of bronchial myofibroblasts in asthma. *Journal of Immunology (Baltimore, Md.: 1950)*, *171*(1), 380-389. https://doi.org/10.4049/jimmunol.171.1.380

Schneider, C. A., Rasband, W. S., & Eliceiri, K. W. (2012). NIH Image to ImageJ : 25 years of image analysis. *Nature Methods*, *9*(7), Article 7. https://doi.org/10.1038/nmeth.2089

Schyns, J., Bai, Q., Ruscitti, C., Radermecker, C., De Schepper, S., Chakarov, S., Farnir, F., Pirottin, D., Ginhoux, F., Boeckxstaens, G., Bureau, F., & Marichal, T. (2019). Non-classical tissue monocytes and two functionally distinct populations of interstitial macrophages populate the mouse lung. *Nature Communications*, *10*(1), 3964. https://doi.org/10.1038/s41467-019-11843-0

Siena, L., Gjomarkaj, M., Elliot, J., Pace, E., Bruno, A., Baraldo, S., Saetta, M., Bonsignore, M. R., & James, A. (2011). Reduced apoptosis of CD8+ T-lymphocytes in the airways of smokers with mild/moderate COPD. *Respiratory Medicine*, *105*(10), 1491-1500. https://doi.org/10.1016/j.rmed.2011.04.014

Smith, T. J., Kahaly, G. J., Ezra, D. G., Fleming, J. C., Dailey, R. A., Tang, R. A., Harris, G. J., Antonelli, A., Salvi, M., Goldberg, R. A., Gigantelli, J. W., Couch, S. M., Shriver, E. M., Hayek, B. R., Hink, E. M., Woodward, R. M., Gabriel, K., Magni, G., & Douglas, R. S. (2017). Teprotumumab for Thyroid-Associated Ophthalmopathy. *The New England Journal of Medicine*, *376*(18), 1748-1761. https://doi.org/10.1056/NEJMoa1614949

Takamura, S., Kato, S., Motozono, C., Shimaoka, T., Ueha, S., Matsuo, K., Miyauchi, K., Masumoto, T., Katsushima, A., Nakayama, T., Tomura, M., Matsushima, K., Kubo, M., & Miyazawa, M. (2019). Interstitial-resident memory CD8+ T cells sustain frontline epithelial memory in the lung. *Journal of Experimental Medicine*, *216*(12), 2736-2747. https://doi.org/10.1084/jem.20190557

Takamura, S., Yagi, H., Hakata, Y., Motozono, C., McMaster, S. R., Masumoto, T., Fujisawa, M., Chikaishi, T., Komeda, J., Itoh, J., Umemura, M., Kyusai, A., Tomura, M., Nakayama, T., Woodland, D. L., Kohlmeier, J. E., & Miyazawa, M. (2016). Specific niches for lung-resident memory CD8+ T cells at the site of tissue regeneration enable CD69-independent

maintenance. *The Journal of Experimental Medicine*, *213*(13), 3057-3073. https://doi.org/10.1084/jem.20160938

Trian, T., Allard, B., Dupin, I., Carvalho, G., Ousova, O., Maurat, E., Bataille, J., Thumerel, M., Begueret, H., Girodet, P.-O., Marthan, R., & Berger, P. (2015). House dust mites induce proliferation of severe asthmatic smooth muscle cells via an epithelium-dependent pathway. *American Journal of Respiratory and Critical Care Medicine*, *191*(5), Article 5. https://doi.org/10.1164/rccm.201409-1582OC

Velotti, F., Barchetta, I., Cimini, F. A., & Cavallo, M. G. (2020). Granzyme B in Inflammatory Diseases : Apoptosis, Inflammation, Extracellular Matrix Remodeling, Epithelial-to-Mesenchymal Transition and Fibrosis. *Frontiers in Immunology*, *11*, 587581. https://doi.org/10.3389/fimmu.2020.587581

Vincenti, F., Rostaing, L., Grinyo, J., Rice, K., Steinberg, S., Gaite, L., Moal, M.-C., Mondragon-Ramirez, G. A., Kothari, J., Polinsky, M. S., Meier-Kriesche, H.-U., Munier, S., & Larsen, C. P. (2016). Belatacept and Long-Term Outcomes in Kidney Transplantation. *The New England Journal of Medicine*, *374*(4), 333-343. https://doi.org/10.1056/NEJMoa1506027

von Andrian, U. H., & Mackay, C. R. (2000). T-cell function and migration. Two sides of the same coin. *The New England Journal of Medicine*, *343*(14), 1020-1034. https://doi.org/10.1056/NEJM200010053431407

Wang, X., Zhang, D., Higham, A., Wolosianka, S., Gai, X., Zhou, L., Petersen, H., Pinto-Plata, V., Divo, M., Silverman, E. K., Celli, B., Singh, D., Sun, Y., & Owen, C. A. (2020). ADAM15 expression is increased in lung CD8+ T cells, macrophages, and bronchial epithelial cells in patients with COPD and is inversely related to airflow obstruction. *Respiratory Research*, *21*(1), 188. https://doi.org/10.1186/s12931-020-01446-5

Williamson, B. D., Carswell, E. A., Rubin, B. Y., Prendergast, J. S., & Old, L. J. (1983). Human tumor necrosis factor produced by human B-cell lines : Synergistic cytotoxic interaction with human interferon. *Proceedings of the National Academy of Sciences*, *80*(17), 5397-5401. https://doi.org/10.1073/pnas.80.17.5397

Wright, J. L., Tai, H., Wang, R., Wang, X., & Churg, A. (2007). Cigarette smoke upregulates pulmonary vascular matrix metalloproteinases via TNF-alpha signaling. *American Journal of Physiology. Lung Cellular and Molecular Physiology*, *292*(1), L125-133. https://doi.org/10.1152/ajplung.00539.2005

Xu, F., Vasilescu, D. M., Kinose, D., Tanabe, N., Ng, K. W., Coxson, H. O., Cooper, J. D., Hackett, T.-L., Verleden, S. E., Vanaudenaerde, B. M., Stevenson, C. S., Lenburg, M. E., Spira, A., Tan, W. C., Sin, D. D., Ng, R. T., & Hogg, J. C. (2021). The molecular and cellular mechanisms associated with the destruction of terminal bronchioles in chronic obstructive pulmonary disease. *European Respiratory Journal*. https://doi.org/10.1183/13993003.01411-2021

Zenke, S., Palm, M. M., Braun, J., Gavrilov, A., Meiser, P., Böttcher, J. P., Beyersdorf, N., Ehl, S., Gerard, A., Lämmermann, T., Schumacher, T. N., Beltman, J. B., & Rohr, J. C. (2020). Quorum Regulation via Nested Antagonistic Feedback Circuits Mediated by the Receptors CD28 and CTLA-4 Confers Robustness to T Cell Population Dynamics. *Immunity*, *52*(2), 313-327.e7. https://doi.org/10.1016/j.immuni.2020.01.018

Appendix 1

Appendix 1—key resources table

Reagent type (species) or resource	Designation	Source or reference	Identifiers	Additional information	RRID
Antibody	Anti-CD8 (rabbit monoclonal)	Fisher Scientific	Cat. #:MA5-14548	IHC (1:200)	AB_10984334
Antibody	Anti-rabbit-HRP	Nichirei Biosciences	Cat. #:414141F	IHC (1:200)	N/A
Antibody	Anti-CD45 (mouse monoclonal)	BD Biosciences	Cat. #:555480	IHC (1:50)	AB_395872
Antibody	Anti-FSP1 (rabbit polyclonal)	Agilent	Cat. #:A5114	IHC (1:200)	AB_2335679
Antibody	Anti-mouse-Alexa568	Fisher Scientific	Cat. #:A-11004	IHC (1:50)	AB_2534072
Antibody	Anti-rabbit-Alexa488	Fisher Scientific	Cat. #:A-11008	IHC (1:200)	AB_143165
Antibody	Anti-LFA-1 (mouse monoclonal)	BioLegend	Cat. #:301233	Blocking experiment (1µg/mL)	AB_2832576
Antibody	Anti-CD54 (mouse monoclonal)	Fisher Scientific	Cat. #:15247027	Blocking experiment (10µg/mL)	N/A
Antibody	Anti-CD86 (mouse monoclonal)	Fisher Scientific	Cat. #:15297097	Blocking experiment (10µg/mL)	N/A
Antibody	Anti-CD44 (rabbit monoclonal)	Fisher Scientific	Cat. #:15266957	Blocking experiment (10µg/mL)	N/A
Antibody	Anti-CXCL8 (recombinant)	BioTechne	Cat. #:MAB208-100	Blocking experiment (1µg/mL)	N/A
Antibody	Anti-CD4-PerCP-Vio700 (recombinant)	Miltenyi Biotec	Cat. #:130-113-228	FC (1 :50)	AB_2726039
Antibody	Anti-CD8-PerCP-Vio700 (recombinant)	Miltenyi Biotec	Cat. #:130-110-682	FC (1 :50)	AB_2659249
Antibody	Anti-CD45RA-FITC (recombinant)	Miltenyi Biotec	Cat. #:130-113-365	FC (1 :50)	AB_2726135
Antibody	Anti-granzyme-APC (recombinant)	Miltenyi Biotec	Cat. #:130-099-780	FC (5 :100)	AB_2651900
Antibody	Anti-TNF- α-PE (recombinant)	Miltenyi Biotec	Cat. #:130-110-066	FC (5 :100)	AB_2654213
Antibody	Anti IFN- γ-APC (recombinant)	Miltenyi Biotec	Cat. #:130-113-496	FC (5 :100)	AB_2751119
Antibody	Anti-IL-17-PE-Cy7 (mouse monoclonal)	Miltenyi Biotec	Cat. #:130-120-413	FC (5 :100)	AB_2752086
Antibody	Anti-IL-10-PE (recombinant)	Miltenyi Biotec	Cat. #:130-112-728	FC (5 :100)	AB_2652318
Antibody	Anti-Collagen Type I-FITC	Sigma Aldrich	Cat. #:FCMAB412F	FC (1:50)	AB_11204160

	(mouse monoclonal)				
Antibody	Anti-CD45-APC (mouse monoclonal)	BD Pharmingen	Cat. #:555485	FC (1 :10)	AB_398600
Antibody	Anti-CXCR1-PE (recombinant)	Miltenyi Biotec	Cat. #:130-115-879	FC (1 :50)	AB_2727234
Antibody	Anti-CXCR2-APC-Cy7 (recombinant)	Miltenyi Biotec	Cat. #:130-119-571	FC (1 :50)	AB_2733103

Acknowledgments

We thank the study participants and the staff of the Thoracic Surgery, Radiology, Pathology, Respiratory, Lung Function Testing departments from the University Hospital of Bordeaux (Bordeaux, France), Isabelle Goasdoue, Isabelle Bernis, Natacha Robert, Virginie Niel, and Marine Servat from the clinical investigation center for technical assistance, and Atika Zouine and Vincent Pitard for technical assistance at the Flow cytometry facility (CNRS UMS 3427, INSERM US 005, Univ. Bordeaux, F-33000 Bordeaux, France), Christel Poujol, Sébastien Marais and Fabrice Cordelières for help with imaging and image analysis et the Bordeaux Imaging Centre (BIC; Bordeaux, France). Microscopy was performed at BIC, a service unit of the CNRS-INSERM and Bordeaux University, a member of the national BioImaging infrastructure of France supported by the French National Research Agency (ANR-10-INBS-04).

Funding: The project was funded by :

the "Fondation de l'Université de Bordeaux" (Fonds pour les maladies chroniques nécessitant une assistance médico-technique FGLMR/AVAD) (ID)

the "Agence Nationale de la Recherche" (ANR-21-CE18-0001-01) (ID)

AstraZeneca (an unrestricted grant to PB).

The COBRA cohort was funded by AstraZeneca, Chiesi, Glaxo-SmithKline, Novartis and Roche.

Author contributions:

Conceptualization: PV, CCB, PB, ID
Software: JMSE, PV, FL
Formal analysis: EE, EM, JMSE, PV, ID
Funding acquisition: ID, PB
Investigation: EE, EM, JMSE, PH, MZ, MT, PV, CCB, ID
Methodology: EE, EM, PH, MZ, PE, TT, JWD, AL, AES, FL, PV, CCB, PB, ID
Project administration: ID
Resources: JMSE, FL, HB, MT, RHC, POG, PB, MZ

Supervision: ID
Validation: EE, EM, PH, PV, CCB, PB, ID
Visualization: EE, EM, JMSE, PH, ID
Writing—original draft: EE, ID
Writing—review & editing: EE, PH, MZ, RM, PV, CCB, PB, ID

Competing interests: PB, POG, ID have a patent (EP N°3050574: Use of plerixafor for treating and/or preventing acute exacerbations of chronic obstructive pulmonary disease) granted. MZ reports personal fees from AstraZeneca, Boehringer Ingelheim, Novartis, Chiesi, GlaxoSmithKline and non-financial support Lilly outside the submitted work; POG reports grants, personal fees and non-financial support from AstraZeneca, personal fees and non-financial support from Chiesi, personal fees and non-financial support from GlaxoSmithKline, personal fees and non-financial support from Novartis, personal fees and non-financial support from Sanofi, outside the submitted work; PB reports grants from AstraZeneca, Glaxo-Smith-Kline, Novartis, Chiesi, which support COBRA during the conduct of the study; grants and personal fees from AstraZeneca, BoehringerIngelheim, Novartis, personal fees and non-financial support from Chiesi, Sanofi, Menarini, outside the submitted work; ID, MZ and PH report grants from the “Fondation Bordeaux Université,” with funding from "Assistance Ventilatoire à Domicile" (AVAD) and "Fédération Girondine de Lutte contre les Maladies Respiratoires" (FGLMR) during the conduct of the study. All other authors declare they have no competing interests.

Materials availability statement: All data needed to evaluate the conclusions are present in the paper, the Supplementary Materials, and/or the deposited data. The customized ImageJ plugin used to perform Delaunay triangulation and cluster quantification is available here:
https://github.com/flevet/Delaunay_clustering_ImageJ
A complete version of the code for launching the simulations associated to control and COPD dynamics can be downloaded from the following site: https://plmbox.math.cnrs.fr/d/49bcbc1db63a4654be7e/